JEM

Article

Transcriptional and functional profiling defines human small intestinal macrophage subsets

Anna Bujko,[1]* Nader Atlasy,[2]* Ole J.B. Landsverk,[1] Lisa Richter,[1] Sheraz Yaqub,[3] Rune Horneland,[4] Ole Øyen,[4] Einar Martin Aandahl,[4,6] Lars Aabakken,[5] Hendrik G. Stunnenberg,[2] Espen S. Bækkevold,[1] and Frode L. Jahnsen[1]

[1]Centre for Immune Regulation, Department of Pathology, University of Oslo and Oslo University Hospital, Rikshospitalet, Oslo, Norway
[2]Department of Molecular Biology, Faculties of Science and Medicine, Radboud Institute of Molecular Life Sciences, Radboud University, Nijmegen, Netherlands
[3]Department of Gastrointestinal Surgery, [4]Department for Transplantation Medicine, and [5]Department for Gastroenterology, Oslo University Hospital, Rikshospitalet, Oslo, Norway
[6]Centre for Molecular Medicine Norway, University of Oslo, Oslo, Norway

Macrophages (Mfs) are instrumental in maintaining immune homeostasis in the intestine, yet studies on the origin and heterogeneity of human intestinal Mfs are scarce. Here, we identified four distinct Mf subpopulations in human small intestine (SI). Assessment of their turnover in duodenal transplants revealed that all Mf subsets were completely replaced over time; Mf1 and Mf2, phenotypically similar to peripheral blood monocytes (PBMos), were largely replaced within 3 wk, whereas two subsets with features of mature Mfs, Mf3 and Mf4, exhibited significantly slower replacement. Mf3 and Mf4 localized differently in SI; Mf3 formed a dense network in mucosal lamina propria, whereas Mf4 was enriched in submucosa. Transcriptional analysis showed that all Mf subsets were markedly distinct from PBMos and dendritic cells. Compared with PBMos, Mf subpopulations showed reduced responsiveness to proinflammatory stimuli but were proficient at endocytosis of particulate and soluble material. These data provide a comprehensive analysis of human SI Mf population and suggest a precursor–progeny relationship with PBMos.

INTRODUCTION

Macrophages (Mfs) are mononuclear phagocytes resident in most tissues where they perform vital functions in defense against pathogens, maintenance of tissue homeostasis, and wound repair (Davies et al., 2013;Varol et al., 2015).Traditionally, peripheral blood monocytes (PBMos) have been viewed as precursors of resident tissue Mfs (van Furth and Cohn, 1968). However, recent studies in mice have demonstrated that in many organs Mfs are populations of self-renewing cells, established before birth from yolk sac– or fetal liver–derived precursors and independent of bone marrow–derived PBMos (Schulz et al., 2012; Hashimoto et al., 2013; Sieweke and Allen, 2013; Hoeffel et al., 2015). Studies on the origin of Mfs in humans are scarce (Haniffa et al., 2009); however, we have reported recently that donor alveolar Mfs in transplanted lungs were maintained for years (Eguíluz-Gracia et al., 2016), indicating that self-renewing resident Mfs also occur in humans.

Mfs in the mouse intestine have been reported to be an exception from this paradigm. It has been shown that during steady-state Ly6C^{hi} PBMos expressing low levels of CX3CR1 constantly migrate to the intestinal lamina propria of mice in a CCR2-dependent manner, where they differentiate into resident mature CX3CR1^{hi} Mfs with antiinflammatory properties through a series of short-lived CX3CR1^{int} intermediaries (Tamoutounour et al., 2012; Bain et al., 2013, 2014).

We have previously shown that the majority of HLA-DR$^+$ mononuclear phagocytes in human small intestine (SI) were mature Mfs expressing CD14, CD68, CD163, and CD209 (DC-SIGN) but negative for CD11c and CCR2, whereas a minor population expressed CD1c and CD11c compatible with being dendritic cells (DCs; Ráki et al., 2006; Beitnes et al., 2011, 2012). A less pronounced population co-expressed CD14 and CD11c, and most of these cells were also CCR2$^+$, indicating that they were recently recruited PBMos (Beitnes et al., 2012). Importantly, the CD11c$^+$CD14$^+$CCR2$^+$ population was selectively expanded in the intestinal mucosa of celiac disease patients after gluten challenge, suggesting that they were increasingly recruited to SI during local inflammation (Beitnes et al., 2012). Moreover, other studies of inflammation in the human gut have shown that recently elicited CD14$^+$ PBMos, in contrast to tissue-resident regulatory Mfs, produce proinflammatory cytokines (Rugtveit et al., 1997; Kamada et al., 2008). However, a comprehensive analysis of Mfs in steady-state human intestine is lacking, and the developmental relationship between PBMos and intestinal Mfs is still unclear.

*A. Bujko and N. Atlasy contributed equally to this paper.

Correspondence to Frode L. Jahnsen: frode.lars.jahnsen@rr-research.no; Anna Bujko: anna.bujko@rr-research.no

The Rockefeller University Press
J. Exp. Med. 2018 Vol. 215 No. 2 441–458
https://doi.org/10.1084/jem.20170057

By extensive phenotyping, transcriptome profiling, and functional analysis of tissue HLA-DR$^+$ mononuclear phagocytes, we demonstrated here that under steady-state conditions human SI harbors four CD14$^+$ Mf subsets that are distinct from DCs. Examining the replacement kinetics of Mfs in transplanted intestine showed that all Mf subsets were replaced by blood-derived precursors within one year after transplantation.

RESULTS

Human SI contains four distinct subsets of Mfs

Flow cytometric analysis of single-cell suspensions from mucosa of duodenal-proximal jejunum (SI) revealed three distinct populations of HLA-DR$^+$CD45$^+$ cells that differentially expressed CD14 and CD11c (Fig. 1 A and Fig. S1 A). CD14$^+$CD11c$^-$ Mfs have been shown to comprise the majority of HLA-DR$^+$ cells in human SI (Beitnes et al., 2011), and the CD14$^+$CD11c$^+$ population was previously shown to expand in patients with celiac disease when challenged with gluten, and based on phenotype it was suggested as deriving from PBMos (Beitnes et al., 2012). We identified two subsets within the CD14$^+$CD11c$^+$ (CD11c$^+$ Mf) gate based on their differential expression levels of HLA-DR and CD14 (Fig. 1 A, top right), whereas two populations could be identified within the CD14$^+$CD11c$^-$ (CD11c$^-$ Mf) gate based on their differential expression of CD11b (Fig. 1 A, bottom right). The subsets were designated Mf1 (CD14$^+$CD11c$^+$HLA-DR^{int}), Mf2 (CD14$^+$CD11c$^+$HLA-DR^{hi}), Mf3 (CD14$^+$CD11c$^-$CD11b$^-$), and Mf4 (CD14^{hi}CD11c$^-$CD11b$^+$). These populations were readily distinguished from DCs that expressed CD11c but not CD14 (Fig. 1 A). Mf3 constituted the majority of CD45$^+$HLA-DR$^+$ cells (median 60.7%), whereas lower numbers of Mf1 (4.7%), Mf2 (11.6%), Mf4 (14.4%), and DCs (5.5%) were found (Fig. 1 B). Both Mf1 and Mf2 populations displayed smaller size and lower autofluorescence than Mf3 and Mf4 and had morphology similar to PBMos, including kidney-shaped nuclei, whereas Mf3 and particularly Mf4 had distinctly shaped nuclei, more cytoplasm, and autofluorescence, characteristic of mature Mfs (Fig. 1, C and D). We then compared phenotypes of SI Mfs and DCs with CD14$^+$ PBMos and blood DCs (PBDCs) by flow cytometry (Fig. 1 E and Fig. S1 B). CD64, MerTK, CD163, CD16, SIRPα, and CD115 were consistently expressed on all four SI Mf subsets, although at varying levels. CX3CR1 was expressed on Mf1, Mf2, and CD14$^+$ PBMos. Low CX3CR1 levels on Mf3 and Mf4 and its expression on a subset of DCs in tissue and blood was consistent with a previous study on skin (McGovern et al., 2014). CD206 was not expressed on CD14$^+$ PBMos and was nearly absent on Mf1, but high levels were detected on the other Mf populations. Intestinal DCs did not express CD163 or CD16 and expressed low levels of CD64, CD115, and MerTK and variable levels of CD11b, SIRPα, CD206, CD1c, and CD103 (Fig. 1 E). Expression of markers on PBDCs was largely similar, although CD163 and CD115 were detected on a subset of PBDCs, and CD206 and CD103 were not expressed (Fig. 1 E). Low levels of CD1c were detected on Mf1 and CD14$^+$ PBMos, as shown previously (Schrøder et al., 2016; Borriello et al., 2017), whereas higher levels were detected on Mf2. CD103 was dimly expressed on a subset of Mf2 (Fig. 1 E), compatible with reported in vitro induction of this marker on PBMos or PBMo-derived DCs by TGF-β and retinoic acid (Schrøder et al., 2016; Roe et al., 2017), which are both abundant in the intestinal mucosa (Hansson et al., 2002; Di Sabatino et al., 2008; Mowat and Agace, 2014).

To control for possible coisolation of PBMos, we performed tissue digestion with the addition of sorted, CFSE-labeled CD14$^+$ PBMos (CFSE-PBMos; Fig. S1 C; McGovern et al., 2014). Flow cytometric analysis of single-cell suspensions showed that CFSE-PBMos and Mf1 exhibited very similar immunophenotypes (Fig. S1 D), but higher expression of HLA-DR, HLA-DQ, CD64, MerTK, CX3CR1, and CD1c on Mf1 indicated that these cells were not PBMos co-isolated during tissue processing.

Human SI Mf compartment comprises short- and long-lived subsets that differ in marker expression

To assess the possibility that PBMos are precursors of intestinal Mfs, we first examined the expression of proteins that have been shown to be differently expressed on PBMos and Mfs (Rugtveit et al., 1996; Beitnes et al., 2012). CCR2 and the antimicrobial protein calprotectin (heterodimer of S100A8 and S100A9) were uniformly expressed by CD14$^+$ PBMos (Fig. 2, A and B). Nearly all Mf1 and Mf2 expressed both proteins, but their mRNA levels were reduced compared with CD14$^+$ PBMos (Fig. 2, A and B). In contrast, only minor fractions of Mf3 and Mf4 expressed these markers (Fig. 2, A and B; and Fig. S2 A). CD209, reported as a marker of mature intestinal Mfs (Ráki et al., 2006), was present on Mf2 and both CD11c$^-$ Mf subsets and was not detected on CD14$^+$ PBMos or Mf1 (Fig. 2 C). However, we observed intermediate levels of *CD209* mRNA in Mf1 (Fig. 2 C).

To directly examine whether human SI Mfs are dependent on PBMo recruitment, we next studied the replacement of duodenal Mfs after combined duodenum–pancreas transplantation in patients with diabetes mellitus (see Materials and methods and Horneland et al. [2015] for details). Relying on a mismatch in HLA class I between donors and recipients, we could accurately determine the degree of chimerism of Mfs in biopsies from donor duodenum obtained 3, 6, and 52 wk after transplantation (Fig. 2 D). Only data from patients with no histological signs of rejection were included. As shown in Fig. 2 E almost all donor Mf1 and Mf2 cells were replaced by recipient cells within 3 wk after surgery, whereas in the CD11c$^-$ Mf compartment only a minor fraction was of recipient origin (median 5.8% Mf3 and 3.4% Mf4). From 3 to 6 wk posttransplantation the fraction of recipient Mf3 and Mf4 increased to 17.7% and 21%, respectively, and at 52 wk

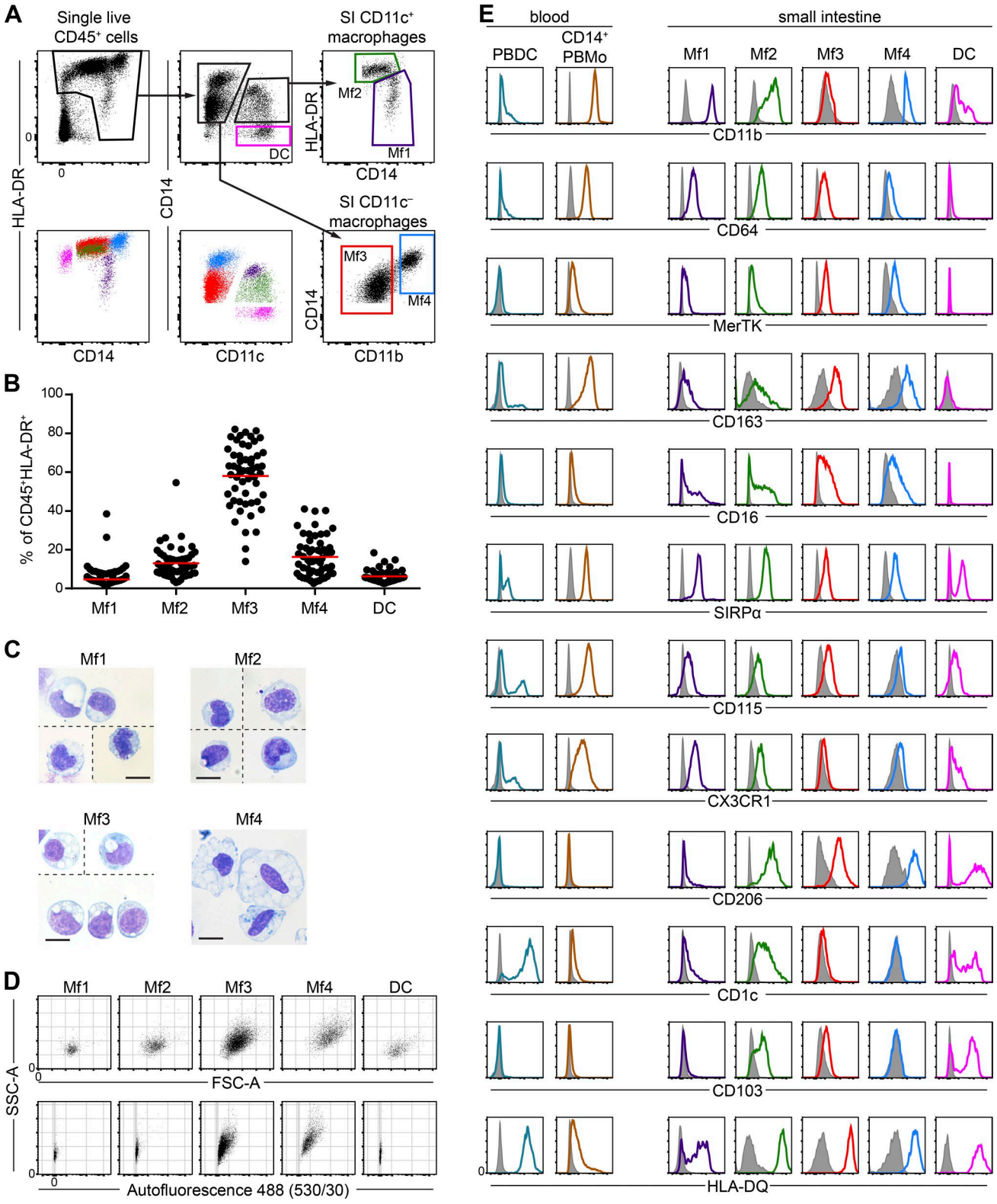

Figure 1. **Human SI contains four distinct Mf subsets. (A)** Representative flow cytometric analysis of human SI Mfs, identifying Mf1 (purple) and Mf2 (green, top right), Mf3 (red), and Mf4 (blue, bottom right), and DCs (pink, top center) among CD45$^+$HLA-DR$^+$ SI mononuclear phagocytes. Arrows indicate sequential gating (see Fig. S1 A for extended gating strategy). Dot plots are representative of all subjects. **(B)** The proportion of SI mononuclear phagocyte subsets given as percentage of all Mfs and DCs (CD45$^+$HLA-DR$^+$) was determined by flow cytometry; bars indicate median values (n = 55). **(C)** Representa-

posttransplantation all donor Mfs were replaced by recipient Mfs. Mf3 and Mf4 showed comparable replacement at the time points analyzed (Fig. S2 B). To determine whether surgical trauma or immunosuppressive regimen could influence Mf replacement, we examined the relative representation of subsets within the Mf compartment after transplantation. We found that at week 3 the proportion of Mf1 was increased with a corresponding reduction of Mf3 (Fig. S2 C). This was most likely the result of increased recruitment of PBMos caused by surgical trauma. Nevertheless, at 6 and 52 wk the cell subset ratios were similar to those observed in normal SI (Fig. 1 B and Fig. S2 C), suggesting that the observed Mf replacement at later time points represented a steady-state situation. Fluorescent in situ hybridization and immunofluorescence (IF) confocal microscopy of donor SI in gender-mismatched patients confirmed a normal distribution of Mfs in donor SI after surgery, as well as the persistence of donor Mfs at week 6 and their complete replacement 1 yr after transplantation (Fig. S2 D).

These experiments showed that human SI Mf compartment, likely derived from PBMos, consisted of short-lived Mf1 and Mf2 subsets and long-lived, more mature Mf3 and Mf4 subsets.

Mature Mf subsets localize to different compartments of the SI

Observed similar replacement rates of Mf3 and Mf4 (Fig. S2 B) suggested that they are not subsequent stages of Mf differentiation but rather represent alternative pathways of Mf2 maturation in the intestine. To further determine the relationship between Mf3 and Mf4 subsets, we investigated their spatial localization in situ by IF microscopy. We observed CD209 expression on the majority of Mfs, but not on DCs (Fig. 2 C and Fig. S3 A; Ráki et al., 2006). $CD209^+$ Mfs were observed throughout the mucosa (Fig. S3 B). $CD209^+CD11b^-$ Mf3 constituted the vast majority of Mfs in the upper crypt area and in the villi, whereas $CD209^+CD11b^+$ Mf4 were mainly situated below the crypts and in the submucosa (Fig. 3, A and B). We also observed $CD209^+$ cells in the crypt area that coexpressed CD11b and CD11c, corresponding to an Mf2 phenotype (Fig. 3 A, inset c). Consistently, by physically separating the tissue at the level of muscularis mucosa before the digestion step, we found that Mf3 cells were enriched in the lamina propria and Mf4 in the submucosa (Fig. 3 C). Moreover, the vast majority of Mfs isolated from the muscle layer situated below the submucosa (muscularis propria) expressed an Mf4 phenotype (Fig. 3 D), indicating that Mf phenotype correlated with tissue localization.

SI Mf subsets are distinguished by their gene expression patterns

To further define the SI Mf subpopulations, we performed low-cell RNA sequencing on sorted tissue Mfs and DCs, as well as $CD14^+$ PBMos isolated from the same donors (n = 5, DCs were sorted from two of these). To effectively compare with Mfs, DCs were sorted into three subpopulations: $CD103^+SIRP\alpha^-$ (single positive; SP-DC), $CD103^+SIRP\alpha^+$ (double positive; DP-DC), and $CD103^-SIRP\alpha^+$ ($CD103^-$ DC; Fig. S4 A), as $CD103^-$ DCs have been shown to be transcriptionally related to $CD14^+$ PBMos (Watchmaker et al., 2014). Principal component analysis (PCA) of all subsets showed three main clusters of non-DC populations separated in component 1 (PC1, 23.35%; Fig. 4 A). $CD14^+$ PBMos clustered separately from all SI Mfs. Mf1 was the Mf subset most similar to $CD14^+$ PBMos, whereas Mf2, Mf3, and Mf4 clustered more together, indicating they were closely related. All DC subsets clustered together and were separated from $CD14^+$ PBMos and Mfs in PC2 (9.24%). $CD14^+$ PBMos pretreated with enzymes to control for effect of tissue digestion (PBMo-lib) clustered with the other $CD14^+$ PBMo samples. We also included PBMo-differentiated Mfs (in vitro Mfs) in our analysis. PCA showed that in vitro Mfs clustered close to Mf1 and distant from the other Mf subsets and DCs (Fig. 4 A). However, in vitro Mfs were distant from Mf1 in PC3 (6.35%; Fig. S4 B). Pearson correlation analysis and hierarchical clustering of the total dataset were consistent with PCA in that $CD14^+$ PBMos formed a separate cluster that displayed the highest degree of correlation with Mf1 among all subpopulations. Mf1 correlated well with Mf2 and less with Mf3 and Mf4. Mf2 essentially coclustered with Mf3 and Mf4. The three DC subsets formed a separate cluster, and DP-DC and $CD103^-$ DC subsets showed some correlation with Mf2 (Fig. 4 B and Fig. S4 C). We validated our SI DC subset dataset by performing gene set enrichment analysis with recently published PBDC and PBMo subpopulation signatures obtained from single-cell RNA sequencing (Villani et al., 2017). This showed that none of the subsets were enriched for PBMo signatures, and SP-DCs were closely related to conventional (c) DC1 whereas DP-DC and $CD103^-$ DC were enriched for genes expressed by cDC2 and cDC1 (Fig. S4 D).

We then performed a polytomous analysis to comprehensively analyze the transcriptomes of the different cell populations in relation to each other (Turro et al., 2011). We used unsupervised hierarchical clustering on the whole dataset to identify top clusters and constructed the associated model matrices for subsequent analysis. By using Bayesian modeling, each gene was assigned to the most probable

tive micrographs of SI Mf subsets sorted by flow cytometry and stained with Hemacolor reagent. n = 2. Bars, 5 µm. **(D)** Representative dot plots showing FSC-A (size), SSC-A (granularity), and autofluorescence of SI Mf subsets and DCs. Autofluorescence was measured as fluorescence excited by a 488-nm laser and collected by a 530/30 bandpass filter, where matched fluorochrome was not included. Data are representative of all subjects. **(E)** Representative flow cytometric staining of surface markers on PBDC, $CD14^+$ PBMo (n = 3 or more; gated as in Fig. S1 B), and SI Mf subsets and DCs (n = 4 or more). Gray histograms represent FMO controls.

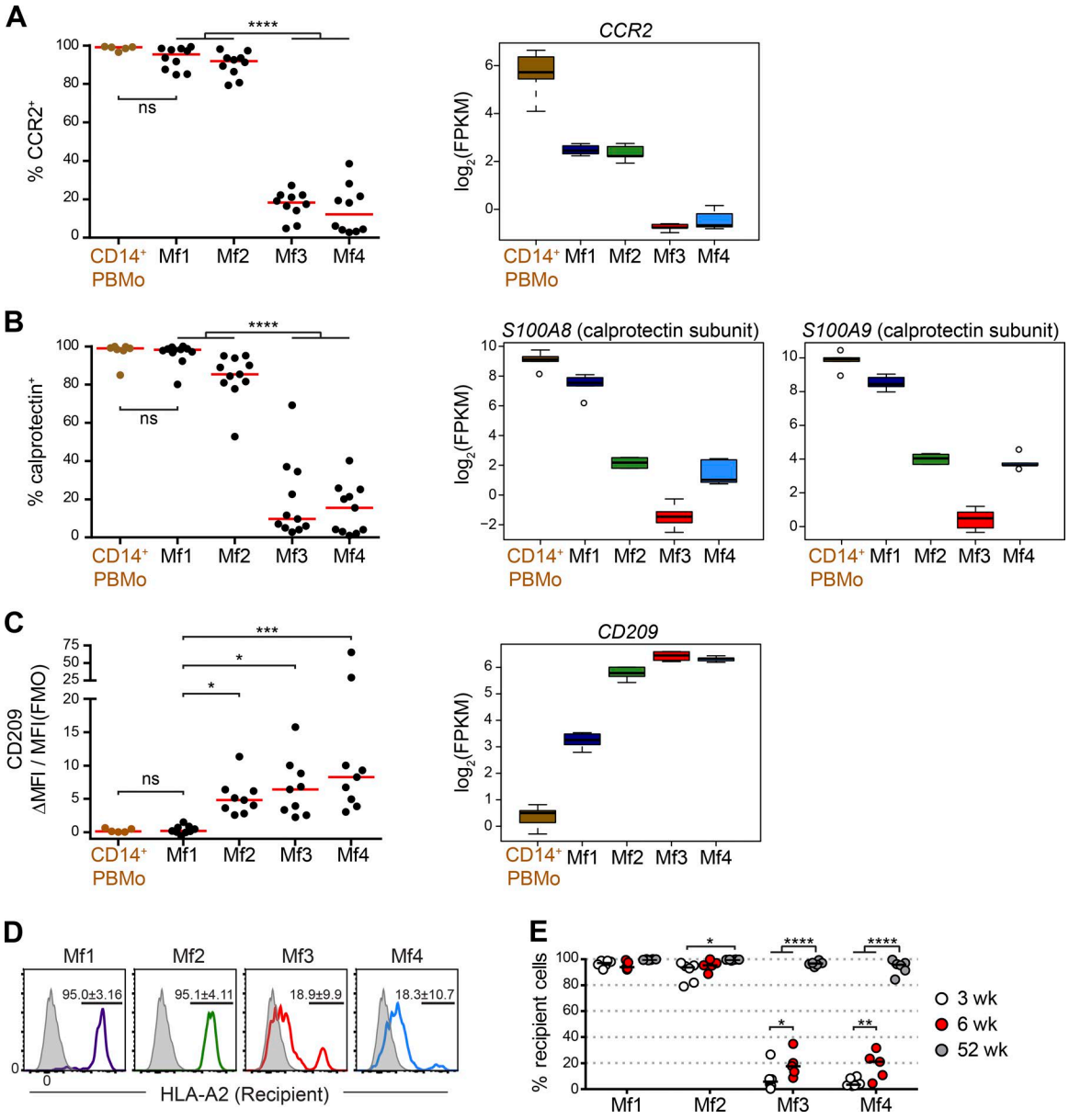

Figure 2. **Human SI Mf compartment comprises short- and long-lived subsets that differ in marker expression. (A)** The percentage of CCR2$^+$ cells among CD14$^+$ PBMo (n = 5) and SI Mf subsets (n = 10) was determined by flow cytometry (left). Gates were set according to FMO controls. The expression of *CCR2* mRNA was determined by RNaseq analysis; n = 5 (right). **(B)** The percentage of calprotectin$^+$ cells among CD14$^+$ PBMo (n = 7) and SI Mf subsets (n = 11) was determined by intracellular staining and flow cytometry. Gates were set according to staining with isotype control antibody. The expression levels of *S100A8* and *S100A9* mRNA were determined by RNaseq analysis; n = 5 (right). **(C)** The median fluorescence intensity (MFI) of CD209 relative to MFI of the FMO control on CD14$^+$ PBMo (n = 5) and SI Mf subsets (n = 9) was determined by flow cytometry. The expression of *CD209* mRNA was determined by RNaseq analysis; n = 5 (right). (A–C, left) Bars represent median values; ns, not significant (t test comparing CD14$^+$ PBMo and Mf1). *, $P < 0.05$; ***, $P < 0.001$; ****, $P < 0.0001$ (RM-ANOVA of SI subsets). (A–C, right) Expression values (log2FPKM) were mean-centered by transcript. **(D)** Representative flow cytometric analysis of recipient-specific HLA-A2 staining on Mf subsets from transplanted duodenum 6 wk after transplantation. Numbers on plots represent recipient$^+$ cells (mean ± SD from all patients analyzed at this time point; n = 5). Gray histograms represent staining of HLA-DR$^+$ stromal cells from the same sample. **(E)** The percentage of recipient-derived cells in each Mf subset at 3 (n = 6), 6 (n = 5), and 52 wk (n = 6) after transplantation was determined by flow cytometry. Bars indicate median values. *, $P < 0.05$; ***, $P < 0.001$; ****, $P < 0.0001$ (two-way ANOVA with RM on population).

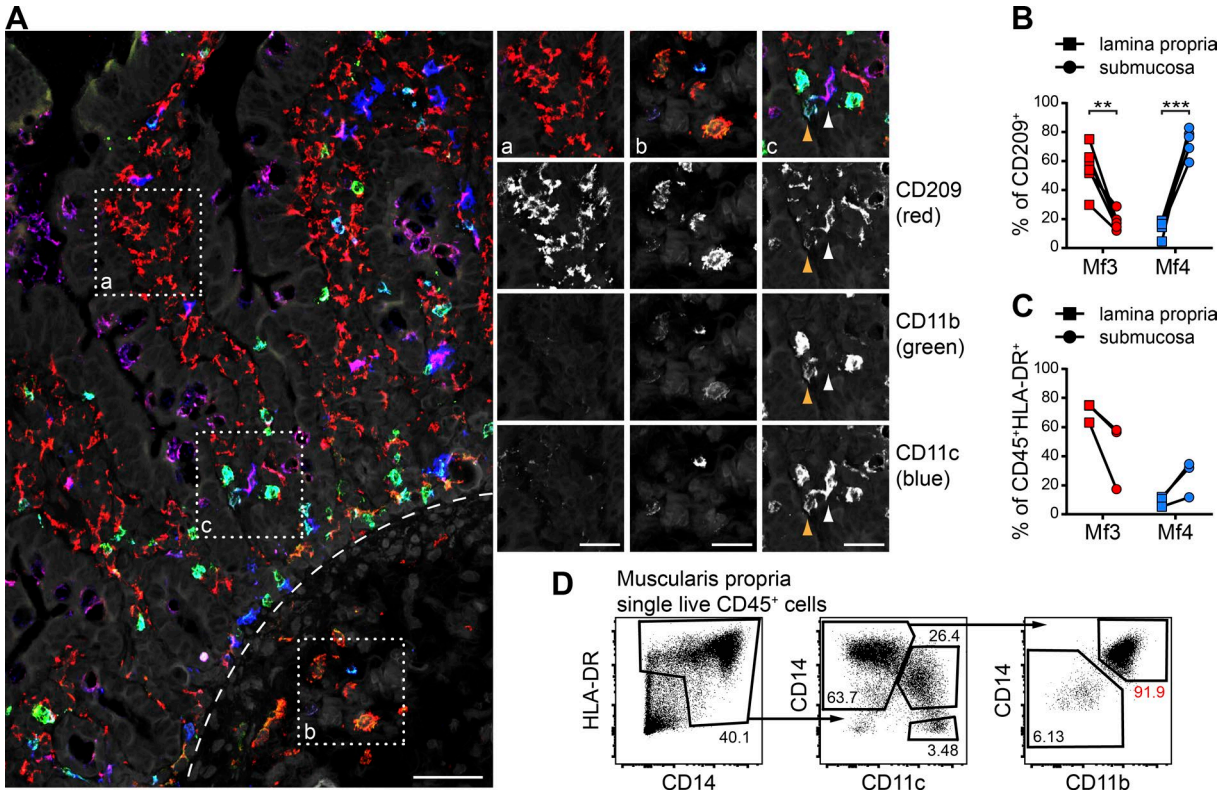

Figure 3. **Mature Mf subsets localize to different compartments of the SI. (A)** IF confocal micrograph from SI stained with CD209 (red), CD11c (blue), CD11b (green), and Hoechst DNA stain (gray). Dashed line marks the border between lamina propria and submucosa; bar, 50 µm. Individual channels from insets a, b, and c are displayed on the right; bars, 25 µm. Arrowheads (inset c) point to $CD209^+CD11c^+CD11b^{hi}$ (orange) and $CD11b^{lo}$ (white) Mf2 cells. The micrograph is representative of six individual subjects. **(B)** The percentage of Mf3 ($CD209^+CD11c^-CD11b^-$) and Mf4 ($CD209^+CD11c^-CD11b^+$) among total $CD209^+$ cells in different compartments of intestinal mucosa as in A ($n = 6$). **, $P < 0.01$; ***, $P < 0.001$ (two-way RM-ANOVA comparing localization). **(C)** The proportion of Mf3 and Mf4 calculated as percentage of all Mfs and DCs ($CD45^+HLA\text{-}DR^+$) was determined by flow cytometry in lamina propria and submucosa separated before the digestion step ($n = 3$). **(D)** Representative flow cytometric analysis of cells isolated from muscularis propria. Arrows indicate sequential gating. Dot plots are representative of five subjects.

model based on the calculated posterior probability (>0.65). We identified in total 6,735 differentially expressed genes for models with a common expression pattern in at least two cell subsets and grouped them by the corresponding model (Fig. 4 C and Tables S1 and S2).

$CD14^+$ PBMos and Mf1 shared the largest number of highly expressed genes (cluster 1, $n = 982$; e.g., *RXRA*, *S100A8*), related to immune effector process and immune response gene ontology (GO) terms, among others (Fig. 4 C and Tables S1 and S2). Cluster 2 contained genes common to Mf2, $CD14^+$ PBMos, and Mf1 ($n = 171$), although these were expressed at lower levels in the former (e.g., *MPO*, *VCAN*) and were related to biological processes corresponding to defense responses including cell activation and secretion. Cluster 3, common to Mf1 and Mf2, included 72 genes (e.g., *FN1*, *SPP1*) involved in cell signaling pathways. Mf1, Mf2, and Mf3 expressed common genes (cluster 4, $n = 207$), including *CCL18* and *CSF3*, related to, e.g., regulations of cell communication and protein phosphorylation. Cluster 5 ($n = 809$) was common to Mf2, Mf3, and Mf4 (e.g., *AHR*, *CFH*, *IL32*) and enriched for genes related to localization and cytokine–cytokine receptor interaction. Cluster 6 ($n = 345$) contained genes expressed in Mf3 and Mf4, which were annotated to terms involved in vesicle mediated transport and FCGR-dependent activation and phagocytosis. Cluster 7 ($n = 365$) comprised genes expressed in Mf1, DC subsets, and to a lesser extent Mf2 (e.g., *RPS20*, *EIF4B*, and many ribosomal protein genes), which were related to translation and RNA processing. Cluster 8 ($n = 783$) contained genes expressed in DC subsets that were associated with cell cycle and mitosis (Fig. 4 C and Tables S1 and S2).

In cluster 9 ($n = 668$), PBMos and Mf1 showed less cell cycle activity compared with other cell types. Several genes involved in the metabolism of carbohydrates were expressed in Mf3, Mf4, and DC subsets (cluster 10, $n = 132$). Clusters 11 and 12 ($n = 29$ and $n = 158$, respectively) comprised genes expressed in $CD14^+$ PBMos, Mf4, and DC subsets, including those involved in chromatin organization (e.g., histone-coding genes). $CD14^+$ PBMos, Mf1, and DC subsets shared cluster 13 ($n = 832$) comprising genes (e.g., *SPI1*,

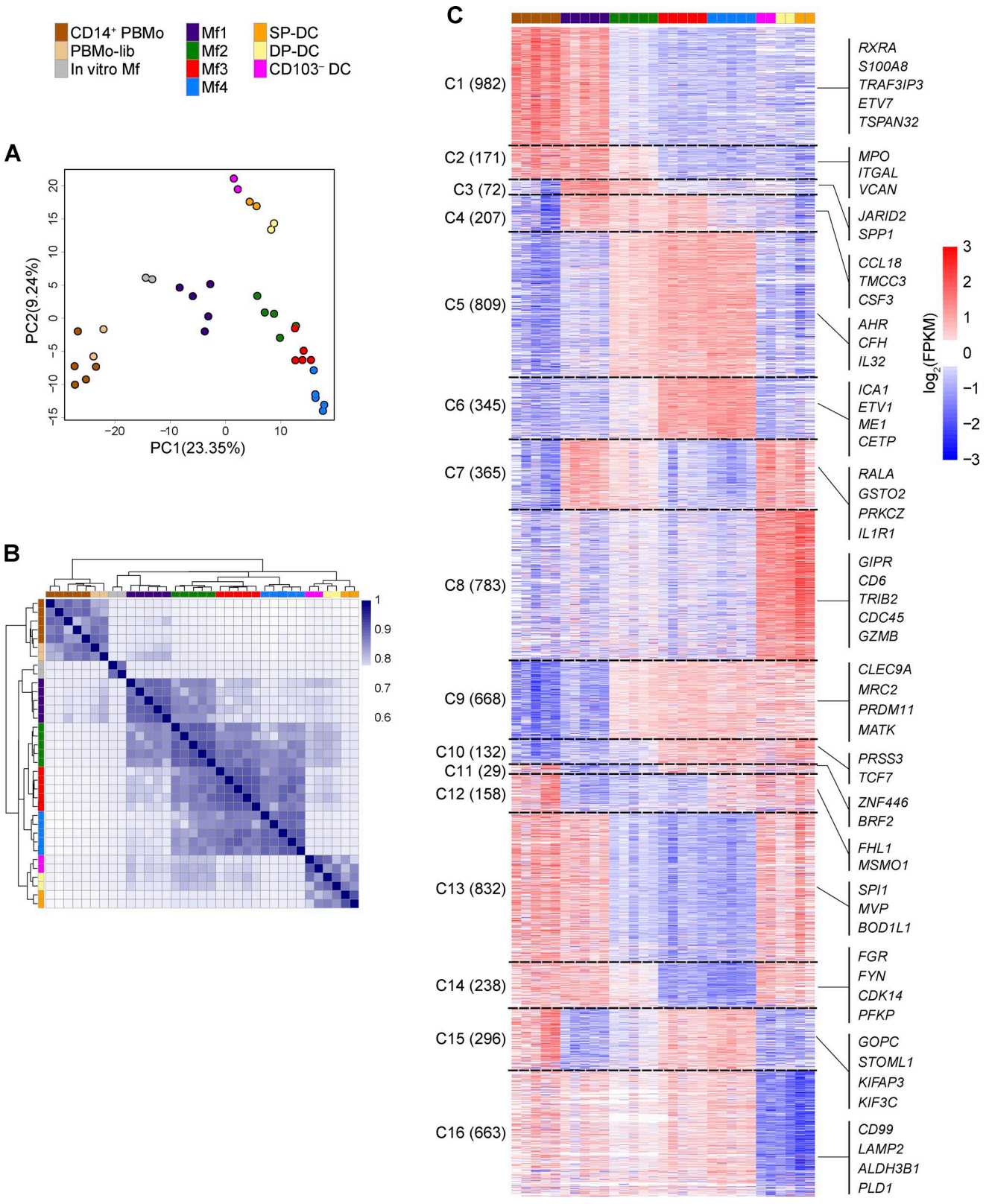

Figure 4. **SI Mf subsets are distinguished by their gene expression patterns. (A)** PCA of top 1,000 differentially expressed genes within CD14⁺ PBMo, PBMo-lib (enzyme-treated CD14⁺ PBMos), SI Mf, and DC subsets and in vitro differentiated Mfs. **(B)** Pearson correlation and hierarchical clustering analysis of CD14⁺ PBMo, PBMo-lib, SI Mf, and DC subsets and in vitro Mfs. Fig. S4 D lists all correlation values. **(C)** Polytomous analysis of differentially expressed

MVP, *BOD1L1*) involved in, e.g., response to hypoxia and many proteasome-related genes. Cluster 14 (n = 238) comprised genes expressed by CD14$^+$ PBMos, Mf1, and DC subsets as well as Mf2 (e.g., *FGR*, *FYN*) related to cell activations processes, whereas CD14$^+$ PBMos, Mf3, and Mf4 expressed genes (cluster 15, n = 296) annotated to GO terms such as cellular localization, organelle organization, and intracellular transport (e.g., *GOPC*, *STOML1*, *KIFAP3*). Lastly, cluster 16 (n = 663) contained genes that were expressed at higher levels in all Mf subpopulations and CD14$^+$ PBMos compared with the DC subsets (e.g., *CD99*, *LAMP2*, *PL1*). These genes were involved in immune effector processes, exocytosis, and lysosomal function (Fig. 4 C and Tables S1 and S2).

Transcriptome profiling showed that SI Mfs comprised subpopulations with complex and partly overlapping expression profiles that were clearly distinct from SI DC subsets, CD14$^+$ PBMos, and in vitro Mfs.

Specific gene expression in SI Mf and DC subsets

Next, we asked whether SI Mfs and DCs expressed subset-specific genes. After determining subset-specific clusters from polytomous analysis for each population, we identified genes expressed at minimum two fragments per kilobase of transcript per million mapped reads (FPKMs) and more than twofold higher than in all other tissue populations. In total 42 genes, including *S100A12*, could be attributed to Mf1 (Fig. 5). By applying these cut-offs, no specific gene signature was found for Mf2, and only two genes were identified for Mf3. For Mf4, we found 32 selectively expressed genes, including *CCL13*, *CCL11*, and several neuron-related genes (*LGI2*, *CCDC141*, *NPTX2*). Interestingly, this population also displayed highest expression of *BMP2* (Table S1), encoding bone morphogenetic protein 2 known to stimulate enteric neurons (Muller et al., 2014). Only a few specific genes were identified for SIRPα$^+$ DC subsets: four genes in DP-DCs and two genes in CD103$^-$ DCs (Fig. 5). Lastly, we found 45 genes specifically expressed in SP-DCs, including cDC1-specific *XCR1* (Fig. 5; Crozat et al., 2010). The relatively few genes specifically expressed in Mf subpopulations further supported that these subsets were closely related.

SI Mfs are highly proficient at antigen uptake

A crucial characteristic of Mfs is clearing debris and pathogens. To assess the ability of Mfs to phagocytose particulate material, we incubated SI cells and PBMCs with pHrodo green-labeled *Escherichia coli* particles. Among SI cells, Mf1 contained the highest percentage of pHrodo$^+$ cells at all time points analyzed, whereas minor differences in phagocytic ability were observed among Mf2, Mf3, and Mf4 populations (Fig. 6 A and Fig. S5 A). All SI Mf subsets were less efficient than CD14$^+$ PBMos but superior to DCs (Fig. 6 A and Fig. S5 A). Pre-incubation of *E. coli* particles with human serum before the assay strongly increased the percentage of pHrodo$^+$ Mfs (opsonized), particularly Mf3 and Mf4, whereas it had little effect on phagocytosis by DCs (Fig. 6 B).

Next, to assess endocytosis and intracellular proteolysis of protein antigens, we incubated cells with fluorochrome-conjugated ovalbumin (DQ-OVA), which emits green fluorescence after proteolysis in lysosomes. Mf1, Mf2, and Mf3 captured and processed DQ-OVA comparably to CD14$^+$ PBMos and better than Mf4 (Fig. 6 C). Tissue-derived DCs appeared to be less efficient than Mfs (Fig. 6 C). Previous studies have shown that ovalbumin can be taken up by several pathways, including mannose receptor (CD206)-mediated endocytosis, scavenger receptor–mediated endocytosis, and pinocytosis (Burgdorf et al., 2007). Analysis of the gene expression data showed that several genes related to endocytosis and lysosomes were differently expressed both among Mf subsets and between Mfs and DCs (Fig. S5 B).

This showed that all Mf subsets can efficiently endocytose both particulate and soluble material and indicated that SI Mfs and DCs may use different pathways for antigen uptake and processing.

SI Mfs have attenuated cytokine production

Mfs can have both immunosuppressive and immune activating properties depending on signals from the microenvironment (Davies et al., 2013). We therefore examined spontaneous and LPS-induced secretion of both proinflammatory and immunosuppressive cytokines and chemokines from sorted CD14$^+$ PBMos, SI Mf subsets, and DCs. Unstimulated Mf1 secreted significantly higher amounts of all cytokines and chemokines compared with the other tissue-derived subsets and CD14$^+$ PBMos (Fig. 7 A). After stimulation with LPS for 21 h, Mf1 further increased secretion of TNFα, IL-1β, IL-6, IL-10, and GM-CSF but produced significantly less CCL2 and IL-8. In contrast, the other subsets showed no significant response to LPS other than an increase in IL-8 production by DCs (Fig. 7 B). The effect of LPS on cytokine secretion by Mf1 was very modest (median fold change of 1.11–1.45 for cytokines with increased secretion, 0.55 for CCL2, and 0.90 for IL-8) and much less pronounced than that observed for LPS-stimulated CD14$^+$ PBMos and PBMo-lib (Fig. 7 C). Pretreating PBMos with Liberase did not affect cytokine secretion (Fig. 7, A and C).

We examined the effect of other TLR ligands by measuring production of TNFα by intracellular flow cytometry after 4 h of stimulation. Consistent with the results above

genes among CD14$^+$ PBMo and SI Mf and DC subsets, grouped into 16 clusters based on top models obtained from unsupervised clustering. Genes were assigned to a model based on the highest calculated posterior probability value (>0.65). Expression values are log2FPKM. Top-ranked genes from each cluster are listed on the right (full list available in Table S1). (A–C) CD14$^+$ PBMos and SI Mfs were isolated from five donors, SI DC subsets from two of these. PBMo-lib were derived from two of the included CD14$^+$ PBMo samples. In vitro Mfs were differentiated from PBMos of two separate healthy donors.

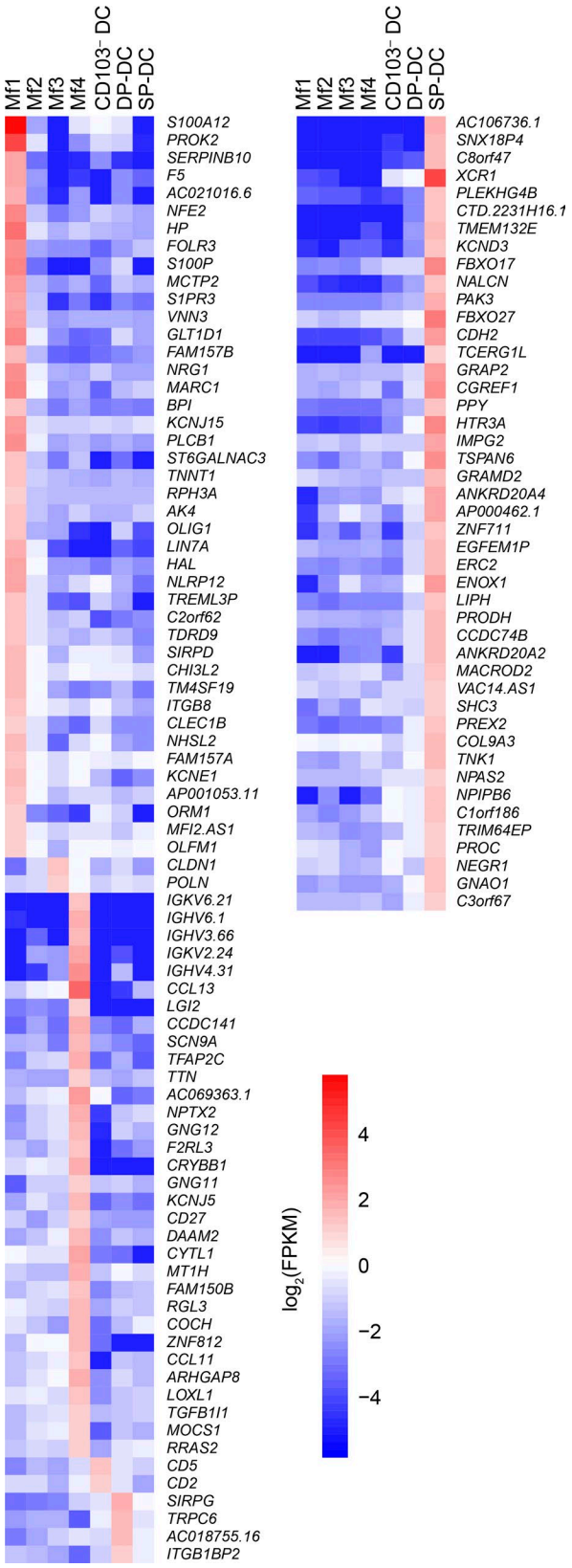

(Fig. 7, A–C), a small fraction of unstimulated Mf1 produced TNFα, which increased significantly in presence of LPS (Fig. 7 D). Similarly, stimulation with poly(I:C), flagellin, and R848 significantly increased the fraction of Mf1 expressing TNFα. Mf2 responded to stimulation to a lesser extent compared with Mf1, whereas Mf3 and Mf4 did not respond to any of the TLR ligands tested (Fig. 7 D).

DISCUSSION

Phenotypic heterogeneity of the Mf compartment has been previously shown in human duodenum (Beitnes et al., 2011, 2012), ileum (Bain et al., 2013), and colon (Ogino et al., 2013). Here, we showed that in human duodenum–proximal jejunum four distinct Mf subpopulations could be identified using only HLA-DR, CD14, CD11c, and CD11b expression. Based on surface marker expression, Mf1 cells were comparable with $CD14^{hi}HLA\text{-}DR^{lo}CD209^{lo}CD163^{lo}$, Mf2 with $CD14^{hi/lo}HLA\text{-}DR^{hi}CD209^{lo}CD163^{lo}CD11c^{+}$, Mf3 with $CD14^{lo}HLA\text{-}DR^{hi}CD209^{hi}CD163^{hi}$, and Mf4 with $CD14^{hi}HLA\text{-}DR^{hi}CD209^{hi}CD163^{hi}$ cells described in terminal ileum (Bain et al., 2013). By using functional and transcriptional analyses, we extended these findings showing that the SI Mf compartment comprised cells with PBMo-like features as well as spatially distinct mature Mf subsets that were hyporesponsive to inflammatory stimuli but highly endocytic.

Studies in mice have shown that PBMos constitutively enter the intestine and replace mature Mfs through a gradual differentiation process (Tamoutounour et al., 2012; Bain et al., 2013; Schridde et al., 2017). In transplanted human duodenum, all Mfs were replaced by recipient cells within one year. Mf1 and Mf2 were most rapidly replaced (most within 3 wk) after transplantation and had a phenotype and morphology that resembled PBMos. However, transcriptional profiling showed that Mf1 were most similar to PBMos whereas Mf2 were more similar to Mf3 and Mf4, indicating that Mf1 were most recently elicited and Mf2 an intermediary differentiation stage between Mf1 and Mf3/4. Mf3 and Mf4 were more slowly replaced in duodenal transplants, had a typical mature Mf morphology, and were more autofluorescent compared with Mf1 and Mf2. Moreover, expression of markers that are typically related to PBMos (CCR2 and calprotectin) and mature Mfs (CD209) was gradational between the Mf subsets. Although we cannot definitively exclude the possibility that circulating precursor cells other than PBMos can give rise to intestinal Mfs in humans, our data suggest that the Mf compartment in human SI comprises a continuum of cells derived from PBMos, differentiating through intermediary Mf1 and

Figure 5. **Specific gene expression in SI Mf and DC subsets.** Mean expression values (log2FPKM) of genes found uniquely in a single SI Mf or DC subset in the polytomous analysis. Genes expressed at minimum 2 FPKM and more than twofold higher than in all other tissue populations were considered specific. SI Mfs were isolated from five donors, SI DC subsets from two of these.

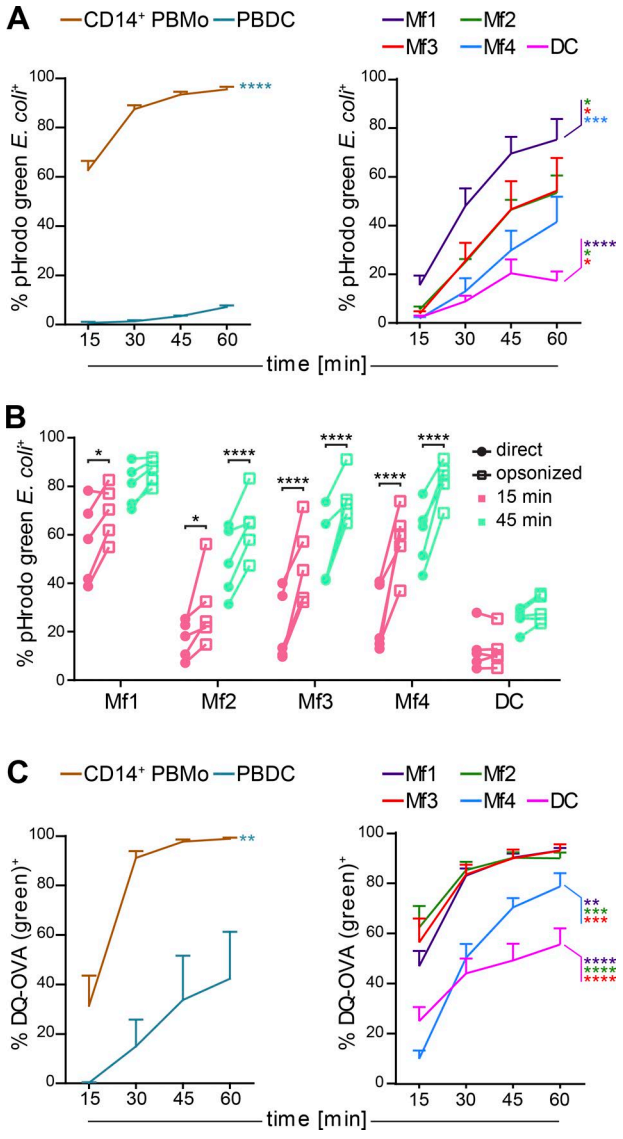

Figure 6. **SI Mfs are highly proficient at antigen uptake. (A)** The percentage of pHrodo green *E. coli*$^+$ cells among CD14$^+$ PBMo, PBDC (left, $n = 5$), and SI Mf subsets and DCs (right, $n = 5$) was determined by flow cytometry after indicated incubation times. **(B)** The effect of pre-incubation with human serum (opsonization) on the uptake of pHrodo green *E. coli* bioparticles by SI Mf subsets and DCs was determined by flow cytometry after 15 or 45 min of incubation ($n = 5$). *E. coli* bioparticles were opsonized by incubating in 50% inactivated human serum for 30 min at 37°C. *, $P < 0.05$; ****, $P < 0.0001$ (two-way RM-ANOVA comparing effect of opsonization at one time point). **(C)** The percentage of DQ-OVA (green)$^+$ cells among CD14$^+$ PBMo, PBDC (left, $n = 5$), and SI Mf subsets and DCs (right, $n = 5$) was determined by flow cytometry after indicated incubation times. (A and C) Data are presented as mean ± SEM of pHrodo$^+$ (A) or DQ-OVA$^+$ (C) cells within each population (Fig. S4 A). Comparisons between subsets are marked in color corresponding to compared subset. *, $P < 0.05$; **, $P < 0.01$; ***, $P < 0.001$; ****, $P < 0.0001$ (two-way RM-ANOVA).

Mf2 into Mf3/4, similar to that reported for Mfs in mouse intestine (Tamoutounour et al., 2012; Bain et al., 2013).

Mf3 and Mf4 were both slowly replaced in duodenal transplants and showed compartmentalized localization in the tissue, suggesting they represented alternative pathways of Mf differentiation in SI. Mf3 comprised the majority of SI Mfs and formed a dense network throughout the villous mucosa, resembling the steady-state resident CX3CR1^{hi} mouse intestinal Mfs (Kim et al., 2011). In contrast, CD11b$^+$ Mf4 were primarily located deep in the mucosa and in the submucosa. Additionally, cells expressing Mf4 phenotype constituted the majority of Mfs in muscularis propria. Submucosa and muscularis propria are densely innervated, and studies in mice have shown that Mfs in muscularis propria are functionally different from lamina propria Mfs and interact with enteric nervous system (Muller et al., 2014; Gabanyi et al., 2016). Moreover, expression of CD11b on microglia has been shown to be important for synaptic pruning (Stephan et al., 2012). Mf4 preferentially expressed *BMP2*, suggesting they may be homologous to mouse muscularis Mfs (Muller et al., 2014).

Mfs and DCs both belong to the mononuclear phagocyte system, share several functional properties (e.g., antigen presentation), and express common surface markers. Consequently, such cells have often been inappropriately identified in the literature (Cerovic et al., 2014; Guilliams and van de Laar, 2015), although recent advancements in fate mapping and tracing experiments have helped define tissue DCs and Mfs in mice (Guilliams et al., 2014; Guilliams and van de Laar, 2015). Our analysis of DC and Mf transcriptomes clearly showed that SI DC subsets were distinct from SI Mf subsets and PBMos. Comparing our data with a recent study on PBDC and PBMo subsets (Villani et al., 2017), we corroborated the findings of Watchmaker et al. (2014) that SP-DCs correlated with cDC1 and DP-DCs with cDC2. In contrast to Watchmaker et al., we did not observe enrichment for PBMo-related gene signatures in CD103$^-$ DCs; however, whether CD103$^-$ DCs included PBMo-derived cells was impossible to determine from these analyses.

Mfs are believed to play an essential role at mucosal sites, both to respond to and eliminate infectious organisms and to maintain homeostasis by clearance of debris and dead cells (Davies et al., 2013). Here we showed that all Mf subsets were very efficient at endocytosis of both particulate and soluble material. Consistently, transcriptional analysis showed that Mf2, Mf3, and Mf4 were enriched for genes involved in endocytosis, receptor-mediated phagocytosis, and lysosome function (clusters 5 and 6). Further, mucosal Mfs were more efficient than DCs in uptake and processing of soluble antigen (ovalbumin). This is consistent with a previous study showing that SI CX3CR1$^+$ Mfs, but not CD103$^+$ DCs, can efficiently capture luminal ovalbumin in mice (Mazzini et al., 2014). SI DCs and Mfs expressed different genes related to endocytosis and lysosome GO terms, which is difficult to correlate with our functional data, but suggests a level of specialization in uptake and processing of antigens between these cell types. In

contrast to previous studies (Smythies et al., 2005; Bain et al., 2013), we observed increased phagocytosis in PBMos compared with SI Mf subsets. This discrepancy may be because of inherent differences between SI and colon Mfs, species, or differences in the method used.

Mf1 secreted low levels of cytokines without stimulation but responded most strongly to TLR ligands among SI subsets. This may suggest that PBMo extravasation through endothelium induces a "poised" state of cellular activation (Takahashi et al., 1996; Williams et al., 2009). Mf1 responded less strongly to LPS stimulation than PBMos, and both spontaneous cytokine production and responsiveness to TLR stimulation were further reduced in Mf2, whereas Mf3 and Mf4 did not respond to any of the TLR ligands tested. This apparent hyporesponsiveness suggests that maturation of Mfs in the intestine could induce an increased threshold for TLR-mediated activation. The poised activation state and opsonization-independent high phagocytic activity of Mf1 suggest their potential role in responding to events that disturb intestinal homeostasis. However, as high levels of proinflammatory cytokines could lead to destruction of tissue integrity (Neurath, 2014), the lack of cytokine production and hyporesponsiveness to stimulation in Mf3 is likely necessary to maintain homeostasis in the intestinal mucosa and an integral part of resident intestinal Mf identity.

An essential role of IL-10 in maintenance of intestinal homeostasis has been demonstrated in studies of *Il10*$^{-/-}$ mice that develop spontaneous enterocolitis (Kühn et al., 1993; Berg et al., 1996; Mao et al., 2012). In humans, the importance of IL-10 is indicated by loss-of-function variants of *IL-10R* that cause severe early-onset inflammatory bowel disease (Glocker et al., 2009; Mao et al., 2012; Shouval et al., 2014). IL-10 can be produced by various leukocytes, including Mfs (Kole and Maloy, 2014). We observed neither spontaneous nor induced IL-10 production in mature SI Mfs, which is consistent with previous studies reporting a lack of IL-10 production by human jejunal Mfs (Smythies et al., 2005, 2010). In contrast, colonic Mfs have been shown to produce IL-10 in humans (Kamada et al., 2008; Ogino et al., 2013) and in mice (Rivollier et al., 2012; Bain et al., 2013; Krause et al., 2015). Because IL-10^{+} Mfs are more frequent in the mouse colon compared with SI (Krause et al., 2015), it is possible that regulation of IL-10 production differs between these compartments. A recent study indicated that the capacity of Mfs to respond to, rather than produce, IL-10 is important to maintain intestinal homeostasis (Zigmond et al., 2014).

Multiple studies probing the function of human Mfs have often used PBMos matured in vitro as surrogates for tissue Mfs. Interestingly, our transcriptional analysis showed that in vitro Mfs separated from all SI Mf subsets. This finding further underscores the importance of microenvironmental factors in differentiation of tissue resident Mfs, especially considering the spectrum of responsiveness of the PBMo-derived cells to various stimuli (Xue et al., 2014). It is likely that PBMo-to-Mf differentiation in the intestinal mucosa involves multiple factors in the microenvironment (Okabe and Medzhitov, 2016; Joeris et al., 2017).

Together, our results support a model where PBMos constitutively migrate into the intestinal mucosa where they gradually lose their proinflammatory capacity and, via sequential short-lived intermediaries (Mf1 and Mf2), differentiate into the mature Mf3 or Mf4, likely depending on tissue-specific signals in the microenvironment. This study provides an important basis for future research on human intestinal Mfs, including their contribution to inflammation, wound healing, and other pathological changes in the intestine.

MATERIALS AND METHODS

Patients

Tissue samples of human SI were obtained from patients with pancreatic cancer, distal bile duct cancer, or periampullary carcinoma undergoing the Whipple procedure (pancreaticoduodenectomy; n = 95, mean age 68 yr, range 39–88 yr, 43 women). Material analyzed was the distal part of resected SI (duodenum–proximal jejunum) from patients without metastases, who had not undergone previous oncological treatment.

Tissue samples from transplanted duodenum were obtained from patients (n = 15) with diabetes mellitus type I who had received pancreas–duodenal segment transplantation either singly or in combination with kidney transplantation. All recipients received standard immunosuppressive regimen (Horneland et al., 2015). Biopsies from donor duodenum were obtained at 3, 6, and 52 wk posttransplantation. Grading of acute cellular rejection was performed at weeks 3 and 6 by an experienced pathologist according to Ruiz et al. (2010), and only patients without signs of cellular rejection were included (n = 11).

Buffy coats and blood were collected from healthy donors and patients undergoing the Whipple procedure.

The study was approved by the Norwegian Regional Committee for Medical Research Ethics, and all patients gave written informed consent.

Tissue handling and cell isolation

Pieces of SI obtained from the Whipple procedure were opened longitudinally and washed in PBS. Mucosa was dissected in narrow strips from underlying fat and muscle tissue and then incubated with shaking in PBS with 2 mM EDTA (Sigma-Aldrich) and 1% FCS (Sigma-Aldrich) three times for 15 min at 37°C. Epithelial cells were removed after each incubation step by filtration through nylon 100-µm mesh. Where stated, after epithelial cell removal, lamina propria was isolated by tearing off of the underlying submucosa under a microscope, and the two compartments were processed separately from this point onward. Tissue was minced and digested with stirring for 60 min in complete RPMI (RPMI1640; Lonza; supplemented with 10% FCS, 1% Pen/Strep; Lonza) containing 0.25 mg/ml Liberase TL (Roche) and 20 U/ml DNase I (Sigma). Digested cell suspension was passed through a

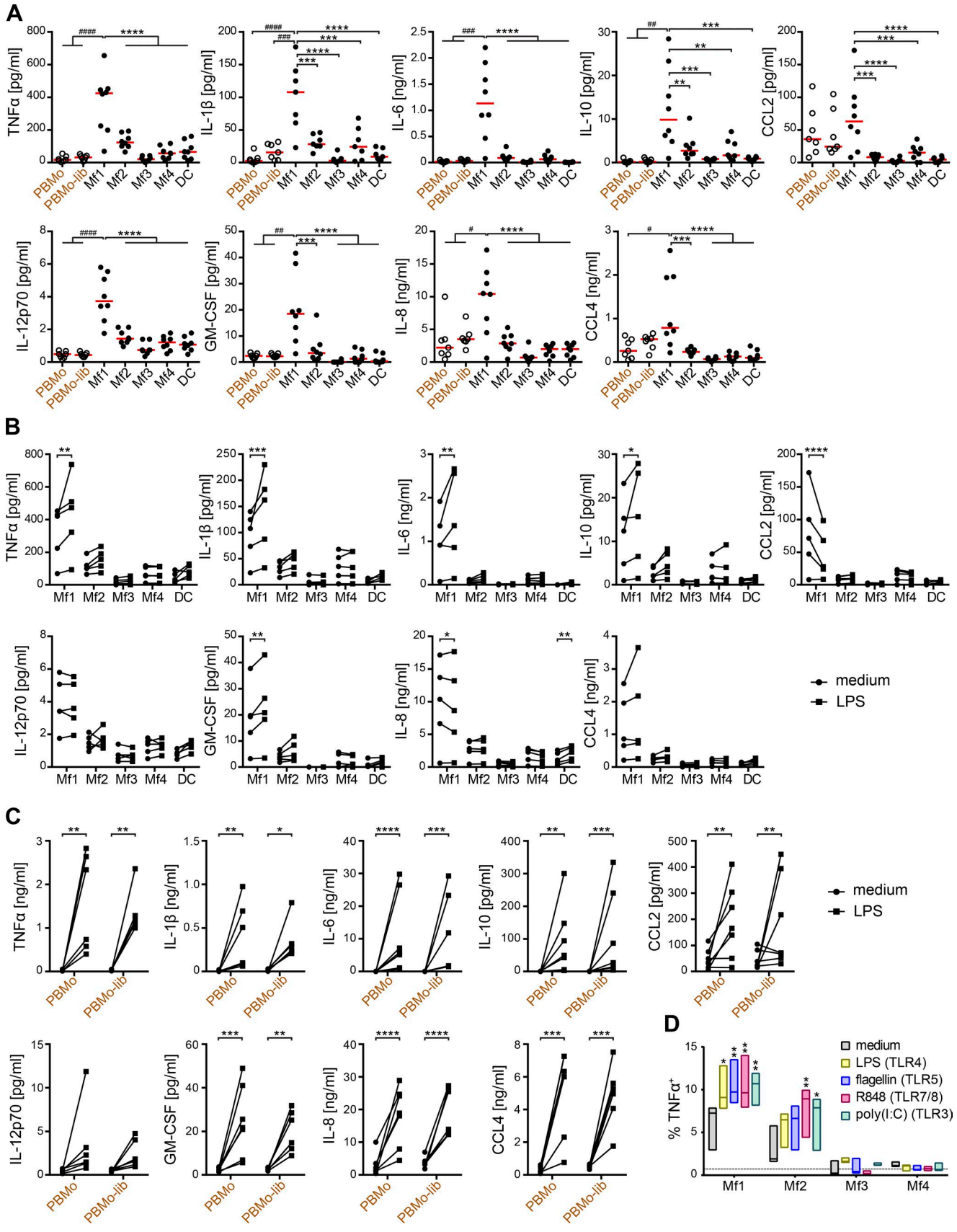

100-µm filter and washed. Mucosal biopsies obtained from transplanted patients were processed according to the same protocol, starting with EDTA washes. Where stated, CFSE-labeled $CD14^+$ PBMos were added to tissue pieces before the digestion step. PBMCs were isolated by density centrifugation over Lymphoprep (Axis-Shield).

Antibodies

The following antibodies were used for flow cytometry. CD1c-PE (L161), CD11b-APC/BV421/BV650 (ICRF44), CD14-APC-Cy7/PacBlue/PE-Cy7/AF700 (HCD14), CD16-PE/AF700 (3G8), CD45-BV510/AF700/APC-Cy7 (HI30), CD64-PE-Cy7 (10.1), CD115-PE (9-4D2-1E4), CD163-APC/PE (GHI/61), SIRPα-PE-Cy7 (SE5A5), CCR2-BV421 (K032C2), CX3CR1-PE (2A9-1), HLA-DQ-FITC/PE (HLADQ1), and HLA-DR-BV605/PerCP-Cy5.5/PE-Cy7 (L243) were from BioLegend. CD11c-PE/APC (S-HCL-3), CD45-APC-H7 (2D1), and CD209-APC (DCN46) were from BD Biosciences. MerTK-PE (125518) was from R&D Systems. CD103-PE (B-Ly7) and TNFα-AF488 (Mab11) were from eBioscience. Calprotectin-PE (MAC387) was from AbD Serotec. Unconjugated CD206 (19.2) was from BD Biosciences and was used with secondary goat anti–mouse IgG1-PE from Southern Biotech. FcR blocking reagent (Miltenyi Biotec) was added with antibodies during staining of surface and intracellular antigens to reduce background staining.

Donor- and recipient-derived cells were distinguished by using HLA-A2-PE (BB7.2) from Abcam, HLA-A3-APC/FITC (GAP.A3) from eBioscience, HLA-B7-PE (BB7.1) from Millipore, and HLA-B8-PE (REA145) from Miltenyi Biotec.

The following unconjugated (unless otherwise stated) primary antibodies were used for microscopy: CD11b (2LPM19c; Thermo Scientific), CD11c (CBR-p150/4G1; AbD Serotec), CD163 (10D6; Leica), CD209-APC (DCN46; BD Biosciences), CD209/DC-SIGN (5D7; Abcam), CD68 (PG-M1; DAKO), and HLA-DRα (TAL.1B5; DAKO). Polyclonal rabbit IgG targeting calprotectin was a gift from I. Dahle (Calpro, Oslo, Norway). The following secondary goat antibodies were used: anti–mouse IgG1-AF488/AF555/AF647, anti–mouse IgG2a-AF555, anti–mouse IgG3-AF594, and anti–rabbit IgG-AF555 (Invitrogen) and anti–mouse IgG2b-AF647, anti–rabbit IgG-AF488, and donkey anti–rabbit IgG-AF647 (Molecular Probes).

Flow cytometry

Cells were stained with fluorescently labeled antibodies (previous section) on ice for 15 min. HLA allotype-specific antibodies were used to distinguish donor and recipient cells in the transplanted intestinal tissue. Donor-specific staining on stromal cells was confirmed in each experiment. Doublets were discriminated in forward scatter area versus height (FSC-A/FSC-H) and side scatter area versus width (SSC-A/SSC-W) plots. Dead cells were excluded based on propidium iodide, TO-PRO-1, or TO-PRO-3 staining (Molecular Probes). BD Cytofix/Cytoperm kit (BD Biosciences) was used for intracellular staining and Foxp3/Transcription Factor Staining Buffer Set (eBioscience) for intranuclear staining, and dead cells were excluded by staining with fixable viability dyes in eFluor 450 or eFluor 780 (eBioscience). Flow cytometry was performed on BD LSRFortessa (BD Biosciences), and data were analyzed with FlowJo software.

Cell sorting

For cytokine immunoassay and morphology assessment, SI cells were first enriched by using 10 µg/ml anti–HLA-DQ antibody (clone FN81; BMA Biomedicals) biotinylated with DSB-X Biotin Protein Labeling kit (Molecular Probes) and Dynabeads FlowComp Flexi kit (Invitrogen). Remaining $CD14^+$ cells were sorted from the $HLA\text{-}DQ^-$ fraction with Dynabeads FlowComp Human CD14 kit (Invitrogen). Bead-free $HLA\text{-}DQ^+$ and $HLA\text{-}DQ^-CD14^+$ cells were stained as described in the previous section, and subpopulations were sorted on FACSAria IIu (BD Biosciences): Mf1 from $HLA\text{-}DQ^-CD14^+$, other Mf subsets and total DCs from $HLA\text{-}DQ^+$ fraction. For cytokine immunoassay and generation of CFSE-monocytes, $CD14^+$ PBMos were sorted from PBMCs (where specified after incubation with Liberase TL and DNase I as described in the Tissue handling and cell isolation section) with CD14 MicroBeads (Miltenyi Biotec). For RNA sequencing, SI cell suspension was first separated with CD14 MicroBeads, and Mf subsets ($n = 5$) were sorted from $CD14^+$ fraction ($0.3–1.25 \times 10^5$ cells per subset) on FACSAria IIu. $CD14^-$ fraction was further enriched for DC by removing $CD3^+$, $CD19^+$, and $CD38^+$ cells by using CD3 Dynabeads (Invitrogen), Pan Mouse IgG Dynabeads (Invitrogen) precoated with unconjugated anti-CD19 (clone HIB19 from BioLegend), and anti-CD38 (clone HB7 from Absolut Antibody LTd) antibodies as described in the Dynabeads

Figure 7. **SI Mfs have attenuated cytokine production. (A)** Spontaneous cytokine release by sorted SI Mf subsets and DCs ($n = 8$) and $CD14^+$ PBMos and PBMo-lib ($n = 7$) was measured by a Bio-Plex assay in supernatants after 21 h of culture. Bars indicate median values. #, $P < 0.05$; ##, $P < 0.01$; ###, $P < 0.001$; ####, $P < 0.0001$ (ANOVA of PBMo, PBMo-lib, and Mf1). **, $P < 0.01$; ***, $P < 0.001$; ****, $P < 0.0001$ (RM-ANOVA of SI subsets). **(B)** Concentration of cytokines released spontaneously (dots) and after stimulation with 1 µg/ml LPS (squares) in supernatants after 21 h of culture of sorted SI Mf subsets and DCs ($n = 5$). *, $P < 0.05$; **, $P < 0.01$; ***, $P < 0.001$; ****, $P < 0.0001$ (two-way RM-ANOVA). **(C)** Concentration of cytokines released spontaneously (dots) and after stimulation with 1 µg/ml LPS (squares) in supernatants after 21 h of culture of sorted $CD14^+$ PBMos and PBMo-lib ($n = 6$ or 7). *, $P < 0.05$; **, $P < 0.01$; ***, $P < 0.001$; ****, $P < 0.0001$ (two-way RM-ANOVA). **(D)** The percentage of $TNF\alpha^+$ cells in SI Mf subsets was determined by intracellular staining and flow cytometric analysis after 4 h of culture in medium only or containing LPS, flagellin, R848, or poly(I:C) ($n = 3$). Floating bars represent range, with a line indicating median. Dotted line represents background staining on Mf3 and Mf4 based on the fraction of cells found within the isotype control gate. *, $P < 0.05$; **, $P < 0.01$ compared with matched medium-only control (two-way RM-ANOVA).

manufacturer's protocol (Direct Technique). 1.15–4.2 × 10^4 cells per DC subset were sorted on FACSAria IIu (n = 2). All cells were sorted into complete RPMI, washed in PBS, then lysed in 80 µl RLT buffer (QIAGEN RNeasy Micro) containing 1% β-mercaptoethanol (Sigma) and stored at −80°C until use. $CD14^+$ PBMos from the same donors were sorted from PBMCs by using the Dynabeads Untouched Human Monocytes kit (Invitrogen) where stated, including enzymatic treatment as in the Tissue handling and cell isolation section. 0.4–1.6 × 10^5 $CD14^+$ PBMos have been lysed in 80 µl RLT buffer containing 1% β-mercaptoethanol and stored at −80°C until use.

Microscopy

To assess morphology, 2.5–5 × 10^4 sorted cells were spun onto a glass slide, fixed, and stained with a Hemacolor stain kit (Merck). Cytospins were viewed by using Olympus BX51 microscope with ColorView IIIu camera (Olympus).

For combined fluorescence in situ hybridization (FISH)/IF, formalin-fixed biopsies were cut at 4 µm, and sections were mounted on slides and incubated overnight at 56°C. Specimens were then dewaxed in xylene, rehydrated in ethanol, and boiled for 20 min in Dako buffer. Sections were incubated with CEP X/Y DNA probes (Abbott Molecular) overnight at 37°C and subsequently stained with antibodies (Antibodies section) according to standard protocol in 1.25% BSA. For IF only, cut sections were boiled in citrate buffer or stained immediately after thawing (sections from cryopreserved biopsies), and staining with secondary antibodies was performed in presence of 10% human serum. Nuclei were counterstained with Hoechst 33258 (Molecular Probes). Images were acquired on an Olympus FV1000 (BX61WI) system with 405-, 488-, 543-, and 633-nm laser lines by using 20×/0.80 or 60×/1.35 UPlanSApo oil objectives (Olympus).

Immunoenzymatic staining for CD209 was performed on formalin-fixed 4-µm sections, dewaxed in xylene and rehydrated in ethanol, by using EnVision FLEX, High pH (Dako Autostainer/Autostainer Plus) and the HRP kit (DAKO), following manufacturer's instructions. In brief, heat-induced antigen retrieval was performed in Tris/EDTA pH9 buffer, followed by peroxidase blocking, staining with primary antibody (anti–DC-SIGN, clone 5D7, 10 µg/ml) for 60 min at room temperature, secondary HRP-conjugated antibody for 30 min at room temperature, and incubation with substrate (DAB) for 7 min at room temperature, with wash steps in between. Slides were then stained with hematoxylin and eosin and scanned by using Pannoramic Midi slide scanner (3DHISTECH).

Cytokine measurement

1.5–3 × 10^4 SI cells or $CD14^+$ PBMos, sorted into populations as described, were cultured in 200 µl complete RPMI in 96-well round bottom plates for 21 h at 37°C with or without 1 µg/ml LPS (Sigma). Cells and debris were removed by centrifugation, and collected supernatants were kept at −80°C until use. Measurement of TNFα, IL-1β, IL-6, IL-8, IL-10, IL-12p70, GM-CSF, CCL2, and CCL4 in culture supernatants was done with a custom premixed Bio-Plex assay (Bio-Rad). Cytokine concentrations in the supernatants were normalized by multiplying the obtained concentrations by a factor equal to 3 × 10^4/x, where x is the number of cells plated in a given well. For flow cytometry assay, 5 × 10^6 SI cells were cultured for 4 h in complete RPMI in ultra-low attach plates and treated with LPS, 1 µg/ml flagellin (InvivoGen), 5 µg/ml poly(I:C) (Sigma), or 1 µg/ml R848 (Tocris Bioscience). Cytokine secretion was blocked with GolgiStop (BD Biosciences) added 30 min after start of the culture.

Assessment of antigen uptake

3 × 10^6 cells were incubated with 50 µg/ml DQ-OVA (Molecular Probes) or with 1 mg/ml pHrodo Green *E. coli* bioparticles (Molecular Probes) for specified times at 37°C or on ice. Where stated, pHrodo Green *E. coli* bioparticles were opsonized by incubation in 50% inactivated human serum for 30 min at 37°C, washed, and resuspended in fresh serum-free buffer before the assay. After incubation, cells were washed, stained with antibodies, and analyzed by flow cytometry by comparing fractions of green fluorescent cells incubated at 37°C and on ice for the same amount of time.

In vitro Mfs

Differentiation was performed as described (Saeed et al., 2014). In brief, buffy coats were obtained from Sanquin in Radboudumc. PBMCs were isolated by double gradient centrifugation, first over Ficoll-Paque Plus (GE Healthcare Life Sciences) and following centrifugation over hyper osmotic Percoll solution (GE Healthcare Life Sciences). T, B, and NK cells were depleted by selection with CD3, CD19, and CD56 MicroBeads on LD columns (Miltenyi Biotec) and PBMos were further enriched by attachment to plastic after culture in RPMI 1640 supplemented with 1% Pen/Strep and 10% human serum (Sigma Aldrich) as a source of M-CSF, for 1 h at 37°C and 5% CO_2 and removal of floating cells. Mfs were obtained after culturing PBMos for 7 d with a change of medium every 3 d.

RNA isolation and library construction

For RNA sequencing SMART-seqII protocol was used as described before (Picelli et al., 2014). In brief, total RNA was isolated by using a column-based kit according to manufacturer's instruction (RNeasy Micro; QIAGEN). RNA with good quality, as assessed by Experion Automated Electrophoresis System (Bio-Rad), was used for cDNA synthesis by using ultra-low input RNA SMART-seq v4 kit according to the manufacturer's protocol (Clonetech). Diagenode Pico sonicator was used to shear cDNA, and the sonication efficiency was evaluated by a 2100 Bioanalyzer (Agilent). A KAPA Hyper Prep kit (KAPA Biosystems) was used to make libraries for next-generation sequencing by using standard Illumina library prep protocol. In brief, sonicated cDNA was end repaired

and A-tailed in one reaction for 30 min at 20°C followed by deactivation of the enzyme by heating to 65°C for another 30 min. Then NextFlex ChIP-seq adapters (Bioo Scientific) were used to barcode the end-repaired A-tailed samples at 20°C for 15 min. Ligated samples were cleaned by using AMPure XP beads (Beckman Coulter) with the sample:bead ratio of 0.8 to remove remaining enzymes and adapters. The libraries were amplified for 10 PCR cycles (HIFI HotStart kit; KAPA), cleaned with QIAquick PCR purification kit (QIAGEN), and subjected to size selection by using the E-Gel electrophoresis system size selection approach (Thermo Fisher Scientific) to select 300 bp fragments. Libraries were concentrated by using vacuum centrifugation (Savant DNA SpeedVac; Thermo). Library concentration was quantified by Qubit 2 (Thermo Fisher Scientific), and the average size of the libraries was determined by the 2100 Bioanalyzer. Sequencing was performed on Illumina NextSeq 500 platform with paired-end reads and a sequencing depth of 35 million reads per end.

Analysis of RNaseq data

Raw data were cleaned from ribosomal RNA contamination by using Bowtie (Langmead and Salzberg, 2012), and the reads with quality score >15 were chosen for subsequent analysis. Processed reads were aligned to human genome (hg19) by using Bowtie (Wu and Nacu, 2010) with default options, and the expression values were used to remove the possible sample batch effects as described before (Leek et al., 2017). The polytomous analysis was performed by using MMSEQ pipeline (Turro et al., 2011) with default options. The functional analysis was performed by using g:Profiler (Reimand et al., 2016). For GO and pathway analysis we used the Gene Ontology consortium database and KEGG and REACTOME databases, respectively. Gene set enrichment analysis was performed by using Broad Institute GSEA software (Mootha et al., 2003; Subramanian et al., 2005). All other analyses were performed in R and Linux.

Statistical analysis

All statistical analyses were performed by using Prism 6.0 (GraphPad Software). Data were analyzed by two-tailed Student's *t* test, Mann-Whitney test, one-way ANOVA (standard, or repeated measures, RM-ANOVA), followed by Tukey's multiple comparison tests, or two-way RM-ANOVA followed by Šídák's multiple comparison tests. Values of $P < 0.05$ were considered significant.

Accession numbers

Sequencing raw data of this study has been deposited under a controlled data access at the European Genome-phenome Archive (http://www.ebi.ac.uk/ega/), which is hosted at the EBI, under accession no. EGAS00001002093.

Online supplemental material

Fig. S1 includes the extended gating of SI Mf subsets and DCs, $CD14^+$ PBMos, and PBDCs, CD14 MicroBeads separation of PBMCs, and phenotype comparison of CFSE-PBMos and Mf1. Fig. S2 (related to Fig. 2) shows phenotype comparison of Mf2, Mf3, and $CCR2^+$ Mf3 fraction and additional data related to Mf replacement, including correlation of Mf3 and Mf4 replacement, representation of Mf subsets in transplant material, and FISH/IF micrographs showing Mf replacement at 6 and 52 wk in sex-mismatched transplanted duodenum. Fig. S3 (related to Fig. 3) shows CD209 expression in SI. Fig. S4 (related to Fig. 4) includes representation of SI DC subsets, PC3 in relation to PC1 and PC2, and gene set enrichment analysis of PBDC and PBMo subset signatures in SI DC subsets. Fig. S5 (related to Fig. 6) explains gating of $pHrodo^+$ populations in uptake assays and includes heatmaps of endocytosis and lysosome-related genes expressed in SI subsets. Table S1 (related to Fig. 4) lists genes included in clusters 1–16. Table S2 (related to Fig. 4) includes GO terms and pathways enriched in clusters 1–16. Tables S1 and S2 are included as Excel files.

ACKNOWLEDGMENTS

The authors thank Kjersti Thorvaldsen Hagen, Aaste Aursjø, and Kathrine Hagelsteen for excellent technical assistance and thank the Flow Cytometry and Confocal Microscopy Core Facilities at Oslo University Hospital, Rikshospitalet.

This study was supported by grants from the Research Council of Norway through its Centres of Excellence funding scheme (179573), and Southern and Eastern Norway Regional Health Authority. H.G. Stunnenberg and N. Atlasy are supported by the Central European University European Research Council Advanced Grant SysStemCell (339431). This work was also backed by the COST Action BM1404 European Network of Investigators Triggering Exploratory Research on Myeloid Regulatory Cells (http://www.mye-euniter.eu), which is supported by the Horizon 2020 - EU Framework Program Research and Innovation Programme.

The authors declare no competing financial interests.

Author contributions: A. Bujko, E.S. Bækkevold, and F.L. Jahnsen conceived the study. A. Bujko, N. Atlasy, and O.J.B. Landsverk designed and performed experiments and analyzed data. L. Richter helped with experiments. S. Yaqub, R. Horneland, O. Øyen, E.M. Aandahl, and L. Aabakken recruited patients and coordinated acquisition of and provided clinical samples. A. Bujko wrote the manuscript. N. Atlasy, O.J.B. Landsverk, H.G. Stunnenberg, E.S. Bækkevold, and F.L. Jahnsen contributed to writing the manuscript. H.G. Stunnenberg, E.S. Bækkevold, and F.L. Jahnsen supervised the study.

Submitted: 10 January 2017
Revised: 28 September 2017
Accepted: 29 November 2017

REFERENCES

Bain, C.C., C.L. Scott, H. Uronen-Hansson, S. Gudjonsson, O. Jansson, O. Grip, M. Guilliams, B. Malissen, W.W. Agace, and A.M. Mowat. 2013. Resident and pro-inflammatory macrophages in the colon represent alternative context-dependent fates of the same Ly6Chi monocyte precursors. *Mucosal Immunol.* 6:498–510. https://doi.org/10.1038/mi.2012.89

Bain, C.C., A. Bravo-Blas, C.L. Scott, E.G. Perdiguero, F. Geissmann, S. Henri, B. Malissen, L.C. Osborne, D. Artis, and A.M. Mowat. 2014. Constant replenishment from circulating monocytes maintains the macrophage pool in the intestine of adult mice. *Nat. Immunol.* 15:929–937. https://doi.org/10.1038/ni.2967

Beitnes, A.C., M. Ráki, K.E. Lundin, J. Jahnsen, L.M. Sollid, and F.L. Jahnsen. 2011. Density of CD163+ CD11c+ dendritic cells increases and CD103+ dendritic cells decreases in the coeliac lesion. *Scand. J. Immunol.* 74:186–194. https://doi.org/10.1111/j.1365-3083.2011.02549.x

Beitnes, A.C., M. Ráki, M. Brottveit, K.E. Lundin, F.L. Jahnsen, and L.M. Sollid. 2012. Rapid accumulation of CD14+CD11c+ dendritic cells in gut mucosa of celiac disease after in vivo gluten challenge. *PLoS One.* 7:e33556. https://doi.org/10.1371/journal.pone.0033556

Berg, D.J., N. Davidson, R. Kühn, W. Müller, S. Menon, G. Holland, L. Thompson-Snipes, M.W. Leach, and D. Rennick. 1996. Enterocolitis and colon cancer in interleukin-10-deficient mice are associated with aberrant cytokine production and CD4(+) TH1-like responses. *J. Clin. Invest.* 98:1010–1020. https://doi.org/10.1172/JCI118861

Borriello, F., R. Iannone, S. Di Somma, V. Vastolo, G. Petrosino, F. Visconte, M. Raia, G. Scalia, S. Loffredo, G. Varricchi, et al. 2017. Lipopolysaccharide-elicited TSLPR expression enriches a functionally discrete subset of human CD14+ CD1c+ monocytes. *J. Immunol.* 198:3426–3435. https://doi.org/10.4049/jimmunol.1601497

Burgdorf, S., A. Kautz, V. Böhnert, P.A. Knolle, and C. Kurts. 2007. Distinct pathways of antigen uptake and intracellular routing in CD4 and CD8 T cell activation. *Science.* 316:612–616. https://doi.org/10.1126/science.1137971

Cerovic, V., C.C. Bain, A.M. Mowat, and S.W. Milling. 2014. Intestinal macrophages and dendritic cells: What's the difference? *Trends Immunol.* 35:270–277. https://doi.org/10.1016/j.it.2014.04.003

Crozat, K., R. Guiton, V. Contreras, V. Feuillet, C.A. Dutertre, E. Ventre, T.P. Vu Manh, T. Baranek, A.K. Storset, J. Marvel, et al. 2010. The XC chemokine receptor 1 is a conserved selective marker of mammalian cells homologous to mouse CD8α+ dendritic cells. *J. Exp. Med.* 207:1283–1292. https://doi.org/10.1084/jem.20100223

Davies, L.C., S.J. Jenkins, J.E. Allen, and P.R. Taylor. 2013. Tissue-resident macrophages. *Nat. Immunol.* 14:986–995. https://doi.org/10.1038/ni.2705

Di Sabatino, A., K.M. Pickard, D. Rampton, L. Kruidenier, L. Rovedatti, N.A. Leakey, G.R. Corazza, G. Monteleone, and T.T. MacDonald. 2008. Blockade of transforming growth factor beta upregulates T-box transcription factor T-bet, and increases T helper cell type 1 cytokine and matrix metalloproteinase-3 production in the human gut mucosa. *Gut.* 57:605–612. https://doi.org/10.1136/gut.2007.130922

Eguíluz-Gracia, I., H.H. Schultz, L.I. Sikkeland, E. Danilova, A.M. Holm, C.J. Pronk, W.W. Agace, M. Iversen, C. Andersen, F.L. Jahnsen, and E.S. Baekkevold. 2016. Long-term persistence of human donor alveolar macrophages in lung transplant recipients. *Thorax.* 71:1006–1011. https://doi.org/10.1136/thoraxjnl-2016-208292

Gabanyi, I., P.A. Muller, L. Feighery, T.Y. Oliveira, F.A. Costa-Pinto, and D. Mucida. 2016. Neuro-immune interactions drive tissue programming in intestinal macrophages. *Cell.* 164:378–391. https://doi.org/10.1016/j.cell.2015.12.023

Glocker, E.O., D. Kotlarz, K. Boztug, E.M. Gertz, A.A. Schäffer, F. Noyan, M. Perro, J. Diestelhorst, A. Allroth, D. Murugan, et al. 2009. Inflammatory bowel disease and mutations affecting the interleukin-10 receptor. *N. Engl. J. Med.* 361:2033–2045. https://doi.org/10.1056/NEJMoa0907206

Guilliams, M., and L. van de Laar. 2015. A hitchhiker's guide to myeloid cell subsets: Practical implementation of a novel mononuclear phagocyte classification system. *Front. Immunol.* 6:406. https://doi.org/10.3389/fimmu.2015.00406

Guilliams, M., F. Ginhoux, C. Jakubzick, S.H. Naik, N. Onai, B.U. Schraml, E. Segura, R. Tussiwand, and S. Yona. 2014. Dendritic cells, monocytes and macrophages: a unified nomenclature based on ontogeny. *Nat. Rev. Immunol.* 14:571–578. https://doi.org/10.1038/nri3712

Haniffa, M., F. Ginhoux, X.N. Wang, V. Bigley, M. Abel, I. Dimmick, S. Bullock, M. Grisotto, T. Booth, P. Taub, et al. 2009. Differential rates of replacement of human dermal dendritic cells and macrophages during hematopoietic stem cell transplantation. *J. Exp. Med.* 206:371–385. https://doi.org/10.1084/jem.20081633

Hansson, T., A.K. Ulfgren, E. Lindroos, A. DannAEus, I. Dahlbom, and L. Klareskog. 2002. Transforming growth factor-beta (TGF-beta) and tissue transglutaminase expression in the small intestine in children with coeliac disease. *Scand. J. Immunol.* 56:530–537. https://doi.org/10.1046/j.1365-3083.2002.01157.x

Hashimoto, D., A. Chow, C. Noizat, P. Teo, M.B. Beasley, M. Leboeuf, C.D. Becker, P. See, J. Price, D. Lucas, et al. 2013. Tissue-resident macrophages self-maintain locally throughout adult life with minimal contribution from circulating monocytes. *Immunity.* 38:792–804. https://doi.org/10.1016/j.immuni.2013.04.004

Hoeffel, G., J. Chen, Y. Lavin, D. Low, F.F. Almeida, P. See, A.E. Beaudin, J. Lum, I. Low, E.C. Forsberg, et al. 2015. C-Myb(+) erythro-myeloid progenitor-derived fetal monocytes give rise to adult tissue-resident macrophages. *Immunity.* 42:665–678. https://doi.org/10.1016/j.immuni.2015.03.011

Horneland, R., V. Paulsen, J.P. Lindahl, K. Grzyb, T.J. Eide, K. Lundin, L. Aabakken, T. Jenssen, E.M. Aandahl, A. Foss, and O. Øyen. 2015. Pancreas transplantation with enteroanastomosis to native duodenum poses technical challenges--but offers improved endoscopic access for scheduled biopsies and therapeutic interventions. *Am. J. Transplant.* 15:242–250. https://doi.org/10.1111/ajt.12953

Joeris, T., K. Müller-Luda, W.W. Agace, and A.M. Mowat. 2017. Diversity and functions of intestinal mononuclear phagocytes. *Mucosal Immunol.* 10:845–864. https://doi.org/10.1038/mi.2017.22

Kamada, N., T. Hisamatsu, S. Okamoto, H. Chinen, T. Kobayashi, T. Sato, A. Sakuraba, M.T. Kitazume, A. Sugita, K. Koganei, et al. 2008. Unique CD14 intestinal macrophages contribute to the pathogenesis of Crohn disease via IL-23/IFN-gamma axis. *J. Clin. Invest.* 118:2269–2280. https://doi.org/10.1172/JCI34610

Kim, K.W., A. Vallon-Eberhard, E. Zigmond, J. Farache, E. Shezen, G. Shakhar, A. Ludwig, S.A. Lira, and S. Jung. 2011. In vivo structure/function and expression analysis of the CX3C chemokine fractalkine. *Blood.* 118:e156–e167. https://doi.org/10.1182/blood-2011-04-348946

Kole, A., and K.J. Maloy. 2014. Control of intestinal inflammation by Interleukin-10. *In* Interleukin-10 in Health and Disease. S. Fillatreau, and A. O'Garra, editors. Springer, Berlin. 19-38.

Krause, P., V. Morris, J.A. Greenbaum, Y. Park, U. Bjoerheden, Z. Mikulski, T. Muffley, J.W. Shui, G. Kim, H. Cheroutre, et al. 2015. IL-10-producing intestinal macrophages prevent excessive antibacterial innate immunity by limiting IL-23 synthesis. *Nat. Commun.* 6:7055. https://doi.org/10.1038/ncomms8055

Kühn, R., J. Löhler, D. Rennick, K. Rajewsky, and W. Müller. 1993. Interleukin-10-deficient mice develop chronic enterocolitis. *Cell.* 75:263–274. https://doi.org/10.1016/0092-8674(93)80068-P

Langmead, B., and S.L. Salzberg. 2012. Fast gapped-read alignment with Bowtie 2. *Nat. Methods.* 9:357–359. https://doi.org/10.1038/nmeth.1923

Leek, J.T., W.E. Johnson, H.S. Parker, E.J. Fertig, A.E. Jaffe, J.D. Storey, Y. Zhang, and L.C. Torres. 2017. sva: Surrogate Variable Analysis. R package version 3.26.0. Available at: http://bioconductor.org/packages/release/bioc/html/sva.html

Mao, H., W. Yang, P.P. Lee, M.H. Ho, J. Yang, S. Zeng, C.Y. Chong, T.L. Lee, W. Tu, and Y.L. Lau. 2012. Exome sequencing identifies novel compound heterozygous mutations of IL-10 receptor 1 in neonatal-onset Crohn's disease. *Genes Immun.* 13:437–442. https://doi.org/10.1038/gene.2012.8

Mazzini, E., L. Massimiliano, G. Penna, and M. Rescigno. 2014. Oral tolerance can be established via gap junction transfer of fed antigens from CX3CR1$^+$ macrophages to CD103$^+$ dendritic cells. *Immunity.* 40:248–261. https://doi.org/10.1016/j.immuni.2013.12.012

McGovern, N., A. Schlitzer, M. Gunawan, L. Jardine, A. Shin, E. Poyner, K. Green, R. Dickinson, X.N. Wang, D. Low, et al. 2014. Human dermal CD14$^+$ cells are a transient population of monocyte-derived macrophages. *Immunity.* 41:465–477. https://doi.org/10.1016/j.immuni.2014.08.006

Mootha, V.K., C.M. Lindgren, K.F. Eriksson, A. Subramanian, S. Sihag, J. Lehar, P. Puigserver, E. Carlsson, M. Ridderstråle, E. Laurila, et al. 2003. PGC-1alpha-responsive genes involved in oxidative phosphorylation are coordinately downregulated in human diabetes. *Nat. Genet.* 34:267–273. https://doi.org/10.1038/ng1180

Mowat, A.M., and W.W. Agace. 2014. Regional specialization within the intestinal immune system. *Nat. Rev. Immunol.* 14:667–685. https://doi.org/10.1038/nri3738

Muller, P.A., B. Koscsó, G.M. Rajani, K. Stevanovic, M.L. Berres, D. Hashimoto, A. Mortha, M. Leboeuf, X.M. Li, D. Mucida, et al. 2014. Crosstalk between muscularis macrophages and enteric neurons regulates gastrointestinal motility. *Cell.* 158:300–313. https://doi.org/10.1016/j.cell.2014.04.050

Neurath, M.F. 2014. Cytokines in inflammatory bowel disease. *Nat. Rev. Immunol.* 14:329–342. https://doi.org/10.1038/nri3661

Ogino, T., J. Nishimura, S. Barman, H. Kayama, S. Uematsu, D. Okuzaki, H. Osawa, N. Haraguchi, M. Uemura, T. Hata, et al. 2013. Increased Th17-inducing activity of CD14+ CD163 low myeloid cells in intestinal lamina propria of patients with Crohn's disease. *Gastroenterology.* 145:1380–91.e1. https://doi.org/10.1053/j.gastro.2013.08.049

Okabe, Y., and R. Medzhitov. 2016. Tissue biology perspective on macrophages. *Nat. Immunol.* 17:9–17. https://doi.org/10.1038/ni.3320

Picelli, S., O.R. Faridani, A.K. Björklund, G. Winberg, S. Sagasser, and R. Sandberg. 2014. Full-length RNA-seq from single cells using Smart-seq2. *Nat. Protoc.* 9:171–181. https://doi.org/10.1038/nprot.2014.006

Ráki, M., S. Tollefsen, Ø. Molberg, K.E. Lundin, L.M. Sollid, and F.L. Jahnsen. 2006. A unique dendritic cell subset accumulates in the celiac lesion and efficiently activates gluten-reactive T cells. *Gastroenterology.* 131:428–438. https://doi.org/10.1053/j.gastro.2006.06.002

Reimand, J., T. Arak, P. Adler, L. Kolberg, S. Reisberg, H. Peterson, and J. Vilo. 2016. g:Profiler-a web server for functional interpretation of gene lists (2016 update). *Nucleic Acids Res.* 44(W1):W83-W89. https://doi.org/10.1093/nar/gkw199

Rivollier, A., J. He, A. Kole, V. Valatas, and B.L. Kelsall. 2012. Inflammation switches the differentiation program of Ly6Chi monocytes from antiinflammatory macrophages to inflammatory dendritic cells in the colon. *J. Exp. Med.* 209:139–155. https://doi.org/10.1084/jem.20101387

Roe, M.M., S. Swain, T.A. Sebrell, M.A. Sewell, M.M. Collins, B.A. Perrino, P.D. Smith, L.E. Smythies, and D. Bimczok. 2017. Differential regulation of CD103 (αE integrin) expression in human dendritic cells by retinoic acid and Toll-like receptor ligands. *J. Leukoc. Biol.* 101:1169–1180. https://doi.org/10.1189/jlb.1MA0316-131R

Rugtveit, J., H. Scott, T.S. Halstensen, J. Norstein, and P. Brandtzaeg. 1996. Expression of the L1 antigen (calprotectin) by tissue macrophages reflects recent recruitment from peripheral blood rather than upregulation of local synthesis: implications for rejection diagnosis in formalin-fixed kidney specimens. *J. Pathol.* 180:194–199. https://doi.org/10.1002/(SICI)1096-9896(199610)180:2<194::AID-PATH628>3.0.CO;2-P

Rugtveit, J., E.M. Nilsen, A. Bakka, H. Carlsen, P. Brandtzaeg, and H. Scott. 1997. Cytokine profiles differ in newly recruited and resident subsets of mucosal macrophages from inflammatory bowel disease. *Gastroenterology.* 112:1493–1505. https://doi.org/10.1016/S0016-5085(97)70030-1

Ruiz, P., H. Takahashi, V. Delacruz, E. Island, G. Selvaggi, S. Nishida, J. Moon, L. Smith, T. Asaoka, D. Levi, et al. 2010. International grading scheme for acute cellular rejection in small-bowel transplantation: Single-center experience. *Transplant. Proc.* 42:47–53. https://doi.org/10.1016/j.transproceed.2009.12.026

Saeed, S., J. Quintin, H.H. Kerstens, N.A. Rao, A. Aghajanirefah, F. Matarese, S.C. Cheng, J. Ratter, K. Berentsen, M.A. van der Ent, et al. 2014. Epigenetic programming of monocyte-to-macrophage differentiation and trained innate immunity. *Science.* 345:1251086. https://doi.org/10.1126/science.1251086

Schridde, A., C.C. Bain, J.U. Mayer, J. Montgomery, E. Pollet, B. Denecke, S.W.F. Milling, S.J. Jenkins, M. Dalod, S. Henri, et al. 2017. Tissue-specific differentiation of colonic macrophages requires TGFβ receptor-mediated signaling. *Mucosal Immunol.* 10:1387–1399. https://doi.org/10.1038/mi.2016.142

Schrøder, M., G.R. Melum, O.J. Landsverk, A. Bujko, S. Yaqub, E. Gran, H. Aamodt, E.S. Bækkevold, F.L. Jahnsen, and L. Richter. 2016. CD1c-expression by monocytes - Implications for the use of commercial CD1c+ dendritic cell isolation kits. *PLoS One.* 11:e0157387. https://doi.org/10.1371/journal.pone.0157387

Schulz, C., E. Gomez Perdiguero, L. Chorro, H. Szabo-Rogers, N. Cagnard, K. Kierdorf, M. Prinz, B. Wu, S.E. Jacobsen, J.W. Pollard, et al. 2012. A lineage of myeloid cells independent of Myb and hematopoietic stem cells. *Science.* 336:86–90. https://doi.org/10.1126/science.1219179

Shouval, D.S., J. Ouahed, A. Biswas, J.A. Goettel, B.H. Horwitz, C. Klein, A.M. Muise, and S.B. Snapper. 2014. Interleukin 10 receptor signaling: master regulator of intestinal mucosal homeostasis in mice and humans. *Adv. Immunol.* 122:177–210. https://doi.org/10.1016/B978-0-12-800267-4.00005-5

Sieweke, M.H., and J.E. Allen. 2013. Beyond stem cells: Self-renewal of differentiated macrophages. *Science.* 342:1242974. https://doi.org/10.1126/science.1242974

Smythies, L.E., M. Sellers, R.H. Clements, M. Mosteller-Barnum, G. Meng, W.H. Benjamin, J.M. Orenstein, and P.D. Smith. 2005. Human intestinal macrophages display profound inflammatory anergy despite avid phagocytic and bacteriocidal activity. *J. Clin. Invest.* 115:66–75. https://doi.org/10.1172/JCI200519229

Smythies, L.E., R. Shen, D. Bimczok, L. Novak, R.H. Clements, D.E. Eckhoff, P. Bouchard, M.D. George, W.K. Hu, S. Dandekar, and P.D. Smith. 2010. Inflammation anergy in human intestinal macrophages is due to Smad-induced IkappaBalpha expression and NF-kappaB inactivation. *J. Biol. Chem.* 285:19593–19604. https://doi.org/10.1074/jbc.M109.069955

Stephan, A.H., B.A. Barres, and B. Stevens. 2012. The complement system: An unexpected role in synaptic pruning during development and disease. *Annu. Rev. Neurosci.* 35:369–389. https://doi.org/10.1146/annurev-neuro-061010-113810

Subramanian, A., P. Tamayo, V.K. Mootha, S. Mukherjee, B.L. Ebert, M.A. Gillette, A. Paulovich, S.L. Pomeroy, T.R. Golub, E.S. Lander, and J.P. Mesirov. 2005. Gene set enrichment analysis: A knowledge-based approach for interpreting genome-wide expression profiles. *Proc. Natl. Acad. Sci. USA.* 102:15545–15550. https://doi.org/10.1073/pnas.0506580102

Takahashi, M., S. Kitagawa, J.I. Masuyama, U. Ikeda, T. Kasahara, Y.I. Takahashi, Y. Furukawa, S. Kano, and K. Shimada. 1996. Human monocyte-endothelial cell interaction induces synthesis of granulocyte-macrophage colony-stimulating factor. *Circulation.* 93:1185–1193. https://doi.org/10.1161/01.CIR.93.6.1185

Tamoutounour, S., S. Henri, H. Lelouard, B. de Bovis, C. de Haar, C.J. van der Woude, A.M. Woltman, Y. Reyal, D. Bonnet, D. Sichien, et al. 2012. CD64 distinguishes macrophages from dendritic cells in the gut and reveals the Th1-inducing role of mesenteric lymph node macrophages during colitis. *Eur. J. Immunol.* 42:3150–3166. https://doi.org/10.1002/eji.201242847

Turro, E., S.Y. Su, Â. Gonçalves, L.J. Coin, S. Richardson, and A. Lewin. 2011. Haplotype and isoform specific expression estimation using multi-mapping RNA-seq reads. *Genome Biol.* 12:R13. https://doi.org/10.1186/gb-2011-12-2-r13

van Furth, R., and Z.A. Cohn. 1968. The origin and kinetics of mononuclear phagocytes. *J. Exp. Med.* 128:415–435. https://doi.org/10.1084/jem.128.3.415

Varol, C., A. Mildner, and S. Jung. 2015. Macrophages: Development and tissue specialization. *Annu. Rev. Immunol.* 33:643–675. https://doi.org/10.1146/annurev-immunol-032414-112220

Villani, A.C., R. Satija, G. Reynolds, S. Sarkizova, K. Shekhar, J. Fletcher, M. Griesbeck, A. Butler, S. Zheng, S. Lazo, et al. 2017. Single-cell RNA-

seq reveals new types of human blood dendritic cells, monocytes, and progenitors. *Science.* 356:eaah4573. https://doi.org/10.1126/science.aah4573

Watchmaker, P.B., K. Lahl, M. Lee, D. Baumjohann, J. Morton, S.J. Kim, R. Zeng, A. Dent, K.M. Ansel, B. Diamond, et al. 2014. Comparative transcriptional and functional profiling defines conserved programs of intestinal DC differentiation in humans and mice. *Nat. Immunol.* 15:98–108. https://doi.org/10.1038/ni.2768

Williams, M.R., Y. Sakurai, S.M. Zughaier, S.G. Eskin, and L.V. McIntire. 2009. Transmigration across activated endothelium induces transcriptional changes, inhibits apoptosis, and decreases antimicrobial protein expression in human monocytes. *J. Leukoc. Biol.* 86:1331–1343. https://doi.org/10.1189/jlb.0209062

Wu, T.D., and S. Nacu. 2010. Fast and SNP-tolerant detection of complex variants and splicing in short reads. *Bioinformatics.* 26:873–881. https://doi.org/10.1093/bioinformatics/btq057

Xue, J., S.V. Schmidt, J. Sander, A. Draffehn, W. Krebs, I. Quester, D. De Nardo, T.D. Gohel, M. Emde, L. Schmidleithner, et al. 2014. Transcriptome-based network analysis reveals a spectrum model of human macrophage activation. *Immunity.* 40:274–288. https://doi.org/10.1016/j.immuni.2014.01.006

Zigmond, E., B. Bernshtein, G. Friedlander, C.R. Walker, S. Yona, K.W. Kim, O. Brenner, R. Krauthgamer, C. Varol, W. Müller, and S. Jung. 2014. Macrophage-restricted interleukin-10 receptor deficiency, but not IL-10 deficiency, causes severe spontaneous colitis. *Immunity.* 40:720–733. https://doi.org/10.1016/j.immuni.2014.03.012